Journal of Volcanology and Geothermal Research 454 (2024) 108182

Contents lists available at ScienceDirect

Journal of Volcanology and Geothermal Research

journal homepage: www.journals.elsevier.com/journal-of-volcanology-and-geothermal-research

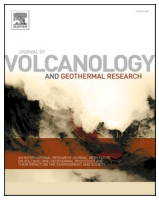

# Event classification, seismicity, and eruption forecasting at Great Sitkin Volcano, Alaska: 1999–2023

J.A. Power [a,*], D.C. Roman [b]

[a] U.S. Geological Survey, Alaska Volcano Observatory, 4230 University Drive, Suite 100, Anchorage, AK 99508, USA
[b] Earth and Planets Laboratory, Carnegie Institution for Science, Washington DC 20015, USA

ARTICLE INFO

*Keywords:*
Great Sitkin Volcano
Aleutians
Average Peak Frequency
Frequency Index
Deep Long-Period seismicity
Bookshelf Fault

ABSTRACT

The frequency content of volcanogenic seismicity is often used to classify events and their spatial and temporal progression is then used to map subsurface volcanic processes. The progression of volcano-seismic events and associated source processes also plays a critical role in eruption forecasting. Here we develop and evaluate a computerized methodology for characterizing volcano-seismic event types using Frequency Index and Average Peak Frequency. We apply and test this technique at Great Sitkin Volcano, Alaska, classifying over 9000 hypocenters between 1999 and 2023. This 24-year time span covers periods of seismic quiescence, earthquake activity on nearby tectonic (bookshelf) faults, precursory unrest from 2016 to 2021, and the explosive onset in May 2021 of the ongoing effusive eruption. We use the spatial and temporal evolution of classified event types to map the active volcanic and tectonic processes, develop a conceptual model of the subsurface magmatic system, and perform a retrospective analysis of eruption forecasts at Great Sitkin Volcano between 2016 and the present. The classification and progression of hypocenters suggests the subsurface Great Sitkin Volcano magmatic system consists of a mid- to lower- crustal source zone between 10 and 40 km depth and an upper crustal magma storage area between −1 and 10 km depth (hypocenter depth is referenced to sea level and negative depths reflect height above sea level). The earliest precursors occurred in July 2016 and consisted of deep long-period and volcano-tectonic earthquakes at mid-crustal depths suggesting the subsequent unrest and eruption were triggered by a deeper intrusion of magma. This mid-crustal seismic activity was immediately followed by the onset upper-crustal long-period events and volcano-tectonic earthquakes VTs suggesting a strong linkage between the shallow and deeper portions of the magmatic system. The upper crustal area was likely capped by the 1974 lava dome until the magmatic explosion on May 26, 2021.

## 1. Introduction

A principal goal of volcanology is to forecast volcanic eruptions in advance and warn of the associated hazards (NASEM, 2017). Forecasts are typically formulated by monitoring multiple geophysical data streams such as seismicity, ground deformation, and gas flux, that are analyzed concurrently in conjunction with satellite and visual observations of the volcano as well as past eruptive behavior. Tracking seismicity is often at the forefront in volcano monitoring and eruption forecasting as it is often the easiest to track in real-time. Precursory seismic unrest may involve a range of signal types including broad spectrum or volcano-tectonic (VT) earthquakes, low-frequency or long-period (LP) events, events with mixed frequencies (hybrid events), and more continuous signals such as volcanic tremor. VT earthquakes are generally thought to reflect shear failure of rock due to stress changes in the crust produced by magma migration (Roman and Cashman, 2006), while LP events are considered to be a consequence of fluid flow (Chouet and Matoza, 2013). Studies of precursory seismicity at numerous volcanoes suggest a typical progression that may include deep (10 to 50 km) VT earthquakes, and deep long-period events DLP events (hypocentral depth greater than 10 km), mid- to shallow-crustal earthquakes surrounding the volcano, and shallow LP and VT earthquakes beneath and within the edifice (Lahr et al., 1994; Benoit and McNutt, 1996; White and McCausland, 2019), although great variability exists from volcano to volcano (e.g. Roman and Cashman, 2018). While closely monitored volcanoes show variation in the strength and timing of precursory signals, volcanologists are developing some insights into the magmatic processes that may govern variations in precursory activity.

* Corresponding author.
*E-mail address:* jpower@usgs.gov (J.A. Power).

https://doi.org/10.1016/j.jvolgeores.2024.108182
Received 5 June 2024; Received in revised form 29 August 2024; Accepted 31 August 2024
Available online 2 September 2024

Recent studies suggest that important controlling factors may include the magma viscosity and mobility within the crust, repose interval between eruptions, and erupted volume (Passarelli and Brodsky, 2012; Rasmussen et al., 2018; Phillipson et al., 2013; Roman et al., 2021). What is becoming apparent is that eruptions at volcanoes that are frequently active or have shallow accumulations of magma and phreatic eruptions have mild precursors and are thus more difficult to forecast than those at volcanoes with longer response intervals and stronger geophysical unrest (Thelen et al., 2010; Cameron et al., 2018; Stix and de Moor, 2018).

A common problem in the long-term (decades: 10 to 50 years) tracking and interpretation of seismic activity are inconsistencies in recording and reporting of seismic observations. The technology involved with instrumentation and telemetry is constantly evolving with recent major shifts from short-period seismometers with analog telemetry to broad-band instruments with digital telemetry. Technology has also advanced seismic data recording over the past several decades from smoked paper and micro-film to continuous digital records. Similarly analytical techniques for identification, location, and characterization of volcanogenic seismicity have also advanced rapidly. Consequently, it can be difficult to assemble consistent sets of seismic observations over periods of years to decades which are often the time scales required to observe and fully characterize subsurface volcanic processes especially at infrequently-active volcanoes.

Our goal in this paper is to develop an automated computerized methodology to characterize the frequency content of located seismic events using both frequency index (FI) (Buurman and West, 2010) and average peak frequency (APF) (Ketner and Power, 2013) that can be applied to long-term volcanic earthquake catalogs and associated digital waveforms. We then apply this automated event classification at Great Sitkin Volcano, located in the Andreanof Islands in the western Aleutian arc (Fig. 1), where the Alaska Volcano Obswervatory (AVO) has operated a six-station seismic network and maintained an earthquake catalog from 1999 to the present (Power et al., 2019). Great Sitkin is a primarily andesitic (silica range 51 to 59 wt% $SiO_2$, Waythomas et al., 2003) volcano that is surrounded by shallow crustal faults (Pesicek et al., 2008; Ruppert et al., 2012). The volcano experienced a protracted five-year period of precursory unrest (2016–2021) that included DLP events, shallow VT earthquakes and LP events, and 15 small explosions between 2017 and 2019. A magmatic eruption began explosively in May 2021 (Orr et al., 2024b) and this has been followed by an extended effusive eruption that continues at present (June 2024). The long-term seismic observations at Great Sitkin Volcano combined with the range, size, and character of eruptive events provides an important case study for seismic forecasting of various styles of volcanic activity (phreatic and magmatic explosions and lava effusion) and the associated seismicity. The seismic analyses presented in this study include development of a one-dimensional seismic velocity model to improve the absolute determination of earthquake hypocenters, automated event classification system using both FI (Buurman and West, 2010) and APF in the spectra (Ketner and Power, 2013), and duration measurements of explosion signals (Searcy and Power, 2020). We use the results of these analyses to evaluate auto-classification of volcano-seismic events, infer the magmatic processes that led to the 2021-present eruptive activity based on the 24+ year record of seismic observations, and develop a conceptual model of the subsurface components of the Great Sitkin magmatic system. We close with a review of forecasts and public warnings issued by the Alaska Volcano Observatory (AVO).

## 2. Background: geology, eruptive history and prior studies

Great Sitkin is a 1714 m high andesitic strato-volcano that is located 35 km northwest of the community of Adak, Alaska (Fig. 1) in the Andreanof Islands. The current volcanic edifice sits on the northwest portion of Great Sitkin Island and is topped by a crater that is roughly 1.3 km in diameter. The northwestern flank of the volcano contains a

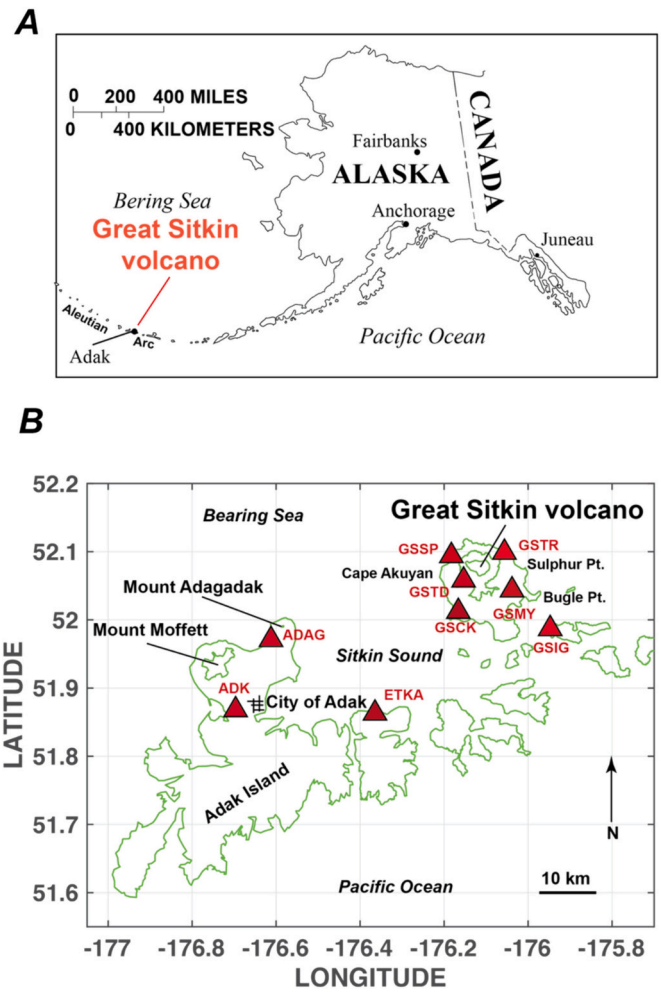


**Fig. 1.** Maps showing the locations of (*A*) Great Sitkin Volcano relative to the state of Alaska and City of Adak and (*B*) the islands, stratovolcanoes, and permanent seismic stations (triangles) near Great Sitkin Volcano.

horseshoe-shaped amphitheater that suggests a large edifice failure that likely occurred in the late Holocene (Waythomas et al., 2003; Coombs et al., 2007). Great Sitkin Volcano is frequently active, with eight reported eruptions since 1792, although many eruptive events may have been missed as a result of its remote location and the persistent cloud cover present in the Aleutian Islands. Miller et al. (1998) reviewed observations of historical eruptions that were reported in 1792, 1828–29, 1904, 1933, 1945, 1946, 1949–50, and 1974. The 1974 eruption was closely observed from Adak (Fig. 1) and apparently began with a large explosion on February 19 that generated an ash plume estimated to have reached altitude of 8.5 km (28,000 ft) above sea level. This explosion was followed by the extrusion of lava that continued until mid-September, forming a dome in the summit crater that was 800 to 900 m in diameter (Waythomas et al., 2003).

Great Sitkin Volcano experienced significant earthquake activity in 2002, focused largely in two off-summit clusters of hypocenters: one centered about 20 km southwest of the summit that began in March and a second about 5 km southeast of the summit that began in May. The largest earthquakes in each cluster were both $M_L$4.3 that occurred on March 18 and May 28, respectively (Moran et al., 2002a, 2002b). Pesicek et al. (2008) developed a three-dimensional velocity model calculated with improved phase arrivals and hypocenters determined through waveform cross-correlation for earthquakes near Great Sitkin Volcano from 1999 through 2005. Their study resolved a low-velocity zone beneath the volcano's summit extending to depths of 10 km and


**Fig. 2.** Photos of Great Sitkin Volcano. (*A*) Great Sitkin Volcano as seen from the Adak airport on May 20, 2021 (photo by Wyatt Mayo), (*B*) steam issuing from the summit crater on November 19, 2017 (photo by Alain Beaupariant), (*C*) Sentinel 2 satellite image showing ash deposit emanating from the summit dome on June 11, 2018, (*D*) ash plume from explosive eruption at 05:03 UTC on May 26, 2021 (photo by Lauren Flynn, U.S. Fish and Wildlife Service), (*E*) steam issuing from the summit lava dome on August 4, 2021 (photo by Dave Ward), and (*F*) oblique aerial photo showing lava flows descending the southwest and south flanks on November 17, 2021 (photo by Angela McConnell).

improved resolution of hypocenters in both clusters. The persistent seismicity beneath the summit was attributed to ongoing magmatic and hydrothermal processes, the southwest cluster to a main-shock/aftershock sequence on a northwest-southeast oriented strike slip fault, and the southeast cluster to either a NW-SE trending fault or the emplacement of magma forming a dike as well as aftershocks of the magnitude 4.3 (Pesicek et al., 2008). Ruppert et al. (2012) suggested that both the southwest and southeast clusters of hypocenters in 2002, as well as similar clusters of hypocenters in this portion of the Aleutian arc, result from slip partitioning in response to the obliquity of the subducting Pacific plate. The oblique component of subduction in this portion of the arc gives rise to block rotation in the forearc (Geist et al., 1988) and arc normal left-lateral strike slip faults along the volcanic axis (Ruppert et al., 2012). Series of well-developed strike-slip faults that are near-orthogonal to the trench are often observed in areas with high obliquity between the overriding and subducted plates and are referred to as

bookshelf faults (e.g. La Femina et al., 2002). Such faults are well developed in areas where oblique subduction is occurring such as Central America (La Femina et al., 2002; Cailleau et al., 2007; Higgins et al., 2022), Sumatra (Sieh and Natawidjaja, 2000), and near Tanaga Volcano that is about 135 km west of Great Sitkin (Lally et al., 2023).

Since the onset of unrest at Great Sitkin, Wang et al. (2023) identified an episode of inflation using Synthetic Aperture Radar (InSAR) data that began in September of 2018, reached a peak rate in September of 2020, and then rapidly diminished until October 2021. This episode of inflation was modeled as a Mogi source centered about 1.7 km southwest of the summit crater at a depth of 5 to 7 km. This was followed by an episode of deflation that began in August of 2021 roughly coincident with an increase in the rate of lava effusion. Analysis of InSAR data between 2002 and 2009 indicates the Great Sitkin edifice did not deform within the resolution of available data during this earlier period (Lu and Dzurisin, 2014). Haney et al. (2022) identified an increase in seismic wave velocities that began in August 2021 when the rate of lava extrusion increased. This increase was centered under the northwest flank of the volcano that had experienced an edifice collapse in the Holocene (Waythomas et al., 2003) and is thought to be more fractured than other portions of the edifice. Using full wave ambient noise tomography, Yang et al. (2023), imaged two low velocity zones roughly three kilometers southwest and five kilometers northwest of the summit and suggested these represent subsurface accumulations of magma.

## 3. Seismic instrumentation and data collection

Seismic monitoring of Great Sitkin Volcano began in the summer of 1999 when AVO deployed five stations (GSTD, GSTR, GSMY, GSSP, and GSCK) on Great Sitkin Island and three additional stations on Igitkin (GSIG), Kagalaska (ETKA) and Adak (ADAG) Islands. An additional station, ADK, on Adak Island operated by the Global Seismic Network was also used to monitor earthquake activity at Great Sitkin (Fig. 1). The Great Sitkin seismic network originally consisted of all 1-Hz vertical component seismometers, except for station GSTD that used a 3-component 2-Hz instrument (Dixon et al., 2003). During the summer of 2019 the Great Sitkin seismic network was upgraded to three-component digital broadband seismometers. Signals from these instruments are transmitted to a central receive site in Adak where they are subsequently relayed to AVO offices in Anchorage, Alaska. Waveforms from detected events are archived at the AVO and continuous data are archived at the EarthScope SAGE/GAGE Data Management Center (DMC). To detect earthquakes at Great Sitkin Volcano the AVO has operated several computerized event detection acquisition systems (Power et al., 2019) and manually determined P- and S-wave arrival times for detected events from 1999 to the present. The results of this effort have been summarized in a series of published catalogs, the most recent of which is by Dixon et al. (2019), and an updated catalog calculated with consistent parameters for earthquake locations and magnitude determination is published in Power et al. (2019). These efforts have resulted in a catalog of 9870 earthquake hypocenters beneath Great Sitkin Volcano (51.9 to 52.2 N and − 175.9 and − 176.4 W) between 1999 and 2023 (Fig. 3). In our study hypocenter depth is referenced to sea level and negative depths reflect height above sea level. All time is referenced to Universal Time Coordinated (UTC).

The Great Sitkin seismic network experienced several outages related to interruptions in electrical power and communications infrastructure in the City of Adak between 1999 and 2023. The most significant of these outages occurred between September 1999 and August 2000, September 2011 and July 2012, December 22, 2018, and March 26, 2019, and April 19 to June 5, 2022. Additionally individual station outages and difficulties with computer hardware occasionally interrupted AVO's ability to preserve waveforms and reliably locate earthquakes at Great Sitkin Volcano between 1999 and 2023. However, the broader seismic network with an additional five seismic stations within 45 km (Fig. 1), allowed AVO to track larger magnitude earthquakes ($M_L$ > 0.5) even when several of the local stations were not operational.

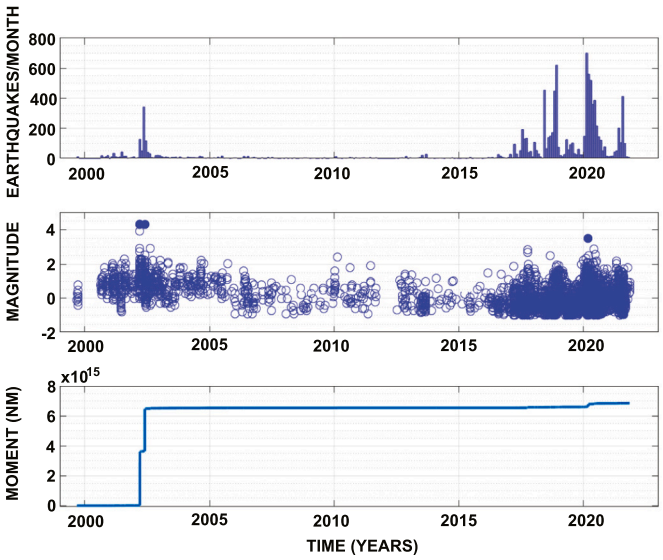


**Fig. 3.** Summary plots of (*A*) number of earthquakes located each month, (*B*) magnitudes of located earthquakes, and (*C*) cumulative moment release at Great Sitkin Volcano from 1999 to 2023. The larger earthquakes that occurred on March 18, 2002 (4.3), May 28, 2002 (4.3) and March 6, 2020 (3.5) and are shown with larger solid symbols.

## 4. Methods and results

### 4.1. Seismic velocity model, earthquake hypocenters, and magnitudes

To improve the absolute earthquake locations relative to those in the AVO catalog we derived a new one-dimensional velocity model and $V_P/V_S$ ratio for Great Sitkin Volcano (Fig. 4 and Table 1). To develop this model, we selected a set of 1768 earthquakes that occurred between January 1, 2013, and October 10, 2021, that had 10 or more P- and S-wave phase readings, azimuthal gap of less than 270 degrees, an epicentral distance of 15 km or less to the nearest station, and a hypocentral depth between 3 km above sea level and 50 km below sea level. We then inverted for the best fit model by perturbing the velocities, layer boundaries, and $V_P/V_S$ using a trial-and-error approach to minimize the RMS (root mean square) through subsequent runs of Hypoinverse (Klein, 2002). These iterations principally involved introducing lower velocity layers on top of the Toth and Kisslinger (1984) model that are thought to be present at Great Sitkin Volcano based on earlier results from (Pesicek et al. (2008): see Fig. 3) and globally by Lasage et al. (2018). We also adjusted the top of the model from 3.2 to 1.7 km above sea level to reflect the height of the volcano. We were not able to refine the velocity structure of Toth and Kisslinger (1984) below depths of about 10 km as too few hypocenters occurred below these depths to accurately characterize the velocities. The best fitting model (Table 1) for our set of 1768 earthquakes uses a $V_P/V_S$ ratio of 1.85 and reduces the RMS of our test set of earthquakes from 0.19 to 0.11. We then relocated the entire Great Sitkin earthquake catalog of 9870 hypocenters from 1999 to 2023 which resulted in a reduction in RMS, GAP (degrees), horizontal (km), and vertical (km) error from 0.15 (±0.07), 162.1 (±56.4), 0.82 (±0.60) and 1.18 (±1.06)) to 0.12 (±0.08), 144.6 (±44.8), 0.59 (±0.69) and 108.0 (±0.53) respectively, where estimated errors within parentheses are the first standard deviation from the mean. See Klein (2002) for formal definitions of error estimates. Earthquake magnitudes were recalculated based on amplitude measurements using Hypoinverse (Klein, 2002) and ranged from −0.9 to 4.3 (Fig. 3).

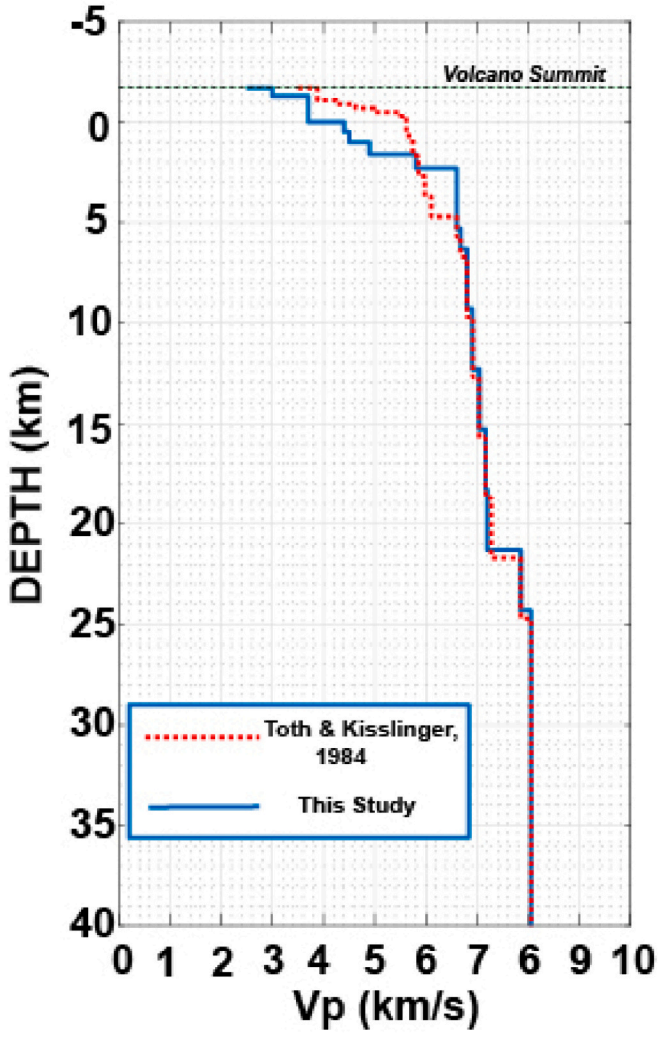


**Fig. 4.** Comparison of one-dimensional velocity models from Toth and Kisslinger (1984) (dotted) and this study (solid). See also Fig. 3 in Pesicek et al. (2008).

**Table 1**
Great Sitkin Volcano P-Wave Velocity Model. Top of model is set at 1.7 km above sea level to match the approximate summit elevation of Great Sitkin Volcano. Numbers is parenthesis reflect depth relative to sea level with negative depths corresponding to height above sea level. This model uses a Vp/Vs ratio of 1.85.

| Velocity (km/s) | Depth (km) |
|---|---|
| 2.5 | 0.0 (−1.7) |
| 3.0 | 0.5 (−1.2) |
| 3.7 | 1.7 (0.0) |
| 4.1 | 2.2 (0.5) |
| 4.5 | 2.7 (1.0) |
| 4.9 | 3.3 (1.6) |
| 5.8 | 4.0 (2.3) |
| 6.6 | 7.0 (5.3) |
| 6.68 | 8.0 (6.3) |
| 6.8 | 11.0 (9.3) |
| 6.92 | 14.0 (12.3) |
| 7.04 | 17.0 (15.3) |
| 7.16 | 20.0 (18.3) |
| 7.28 | 23.0 (21.3) |
| 8.05 | 40.0 (38.7) |

### 4.2. Event classification

To consistently characterize the frequency content of the waveforms for located seismic events at Great Sitkin Volcano, we have developed a computer algorithm that extracts frequency parameters from the recorded waveforms and calculates the frequency index (FI) (Buurman and West, 2010) and the average peak frequency (APF) (Ketner and Power, 2013) of the first five peaks in the stacked spectrum from the three closest stations to the epicenter. We use this code to assign the FI and APF values to the 9870 located events in the AVO catalog within about 20 km of the summit of Great Sitkin between 1999 and 2023. To describe the frequency content of located events in this manuscript we generally use the terminology developed by Lahr et al. (1994) and describe events as volcano-tectonic (VT) earthquakes and long-period (LP) events. The definition of these terms is not entirely consistent in the literature and are often used inter-changeably with other terminology such as high-frequency (HF), low-frequency (LF) and brittle failure. Although classification of intermediate (e.g. 'hybrid events'; Lahr et al., 1994) may be appropriate, we choose a simple binary classification scheme in which we consider LPs to have dominant frequencies at 1–5 Hz and VTs to have dominant frequencies at 6–10 Hz (Fig. 5), to limit subjectivity in defining event classes. We also use the term "deep long-period event (DLP)' to describe LP events that occur at hypocentral depths greater than 10 km after Power et al. (2004). While developing and testing our classification algorithm we use a simple binary classification for FI values above and below zero and refer to events as LP or VT. In the analysis and discussion sections we use the FI value that places the classification on a spectrum or scale and provides greater distinction of frequency content.

For these calculations we used event-detected waveform files archived at AVO for events between 1999 and 2006 and waveforms extracted from the EarthScope DMC for events between 2006 and 2023. To provide consistency throughout the study period we down sampled the short-period data collected at 100 Hz between 1999 and 2019 to 50 Hz to match the data collected after the network was upgraded to digital broadband instruments. The selected waveforms were demeaned,

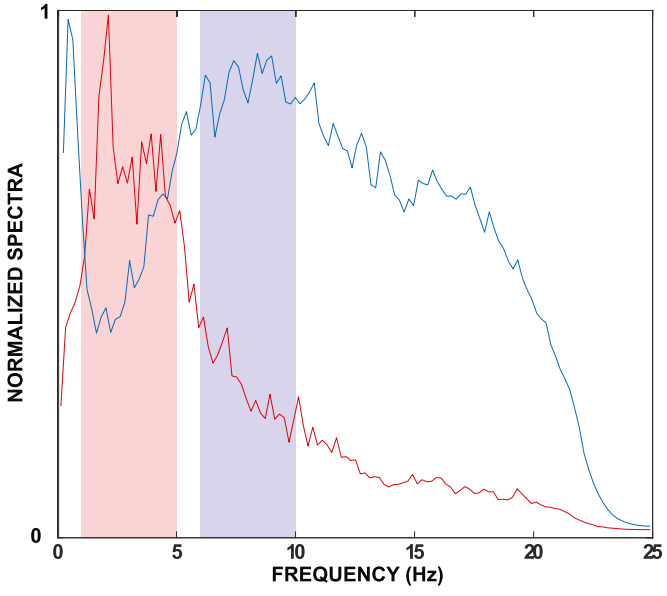


**Fig. 5.** Stacked frequency spectra for LP and VT waveforms verified through manual classification. Red line: Stacked frequency spectrum for 152 manually-verified LP events. Blue line: Stacked frequency spectrum for 323 manually-verified VT earthquakes. Amplitude for both stacked spectra area normalized to 1 for comparison. For FI calculation, the red shaded area indicates $A_{lower}$ and the blue shaded area shows $A_{upper}$. (For interpretation of the references to color in this figure legend, the reader is referred to the web version of this article.)

detrended, and we applied a hamming taper prior to applying a second order Butterworth bandpass filter between 0.5 and 20 Hz. This algorithm then selects a five second window starting at the manually determined P-wave arrival time for the three stations with the earliest arrivals and calculates a 125-point Power Spectrum Density (PSD). We then calculate the frequency index (FI) using two frequency bands ($A_{Lower}$ = 1–5 Hz and $A_{upper}$ = 6–10 Hz) following the methodology developed by (Buurrman and West, 2010) and determine the five highest peaks in the stacked spectra in a manner similar to that described by Ketner and Power (2013); the average peak frequency (APF) is simply the mean of these five peaks.

To aid in assessing the quality of the automated FI classifications (i.e., the extent to which they are influenced by factors such as low-frequency microseismic noise and local station effects) we also calculated the kurtosis and skewness of the stacked PSD between 1 and 10 Hz for all events. The skewness ('symmetry') and kurtosis ('peakedness') provide a simple quantitative description of the shape of the stacked spectrum that may act as a simple basis for identifying events whose stacked spectrum is dominated by low-frequency microseismic noise (Figs. 6–8).

To determine the accuracy of FI event classifications and appropriate criteria for determining well- vs poorly-autoclassified events, we manually classified a subset of the events as follows:

- We randomly selected 718 events from the full autoclassified dataset.
- Both authors independently classified all events in this subset manually by inspecting the bandpassed waveforms and their individual spectrograms, and the individual and stack spectra (blind to the assigned auto classification) and assigning a class of 'High-Frequency,' 'Low-Frequency,' or 'Uncertain.'
- If the two independent manual classifications agreed, the event was assigned a manual class. If the two independent manual classifications disagreed, or if one author assigned an 'uncertain' class, the event was not manually classified (assigned an 'Uncertain' class)
- Based on this exercise, 353 of the test events were manually classified as VT or 'High-Frequency,' 158 were manually classified as LP or 'Low-Frequency,' and 207 were assigned an 'Uncertain' manual classification.
- The manual classification was then compared to the autoclassification (Fig. 9) to assess the appropriate criteria for accepting an autoclassification for the full data set.

Based on this verification exercise (Fig. 9), we find that our autoclassification algorithm always identifies VT earthquakes (i.e., no blue crosses in LF columns in Fig. 9) correctly with FI values above zero. However, we find that some true VT earthquakes (as indicated by manual classifications) are incorrectly autoclassified as LPs (red crosses shaded by gray boxes in HF columns in Fig. 9). Based on the characteristics of the incorrectly-autoclassified events in our test data set, we define the following quality criteria for assessing the full set of event FI autoclassifications: (1) We accept any auto classified VT earthquake as accurate. (2) Good LP classifications occur when FI is below −0.2, magnitude above −0.3, kurtosis below 7.0, and Skewness below 2. (3) Events that do not meet these criteria are assigned an 'uncertain' autoclassification in the remainder of our analyses below.

To evaluate the classification using average peak frequency (APF) we have plotted our FI values versus the values determined for APF (Fig. 10). A linear regression returns a slope of 8.16, a y-intercept of 5.13, and an R-squared value of 0.84 indicating that our calculated values for FI and APF track well. APF values above 5.13 should roughly

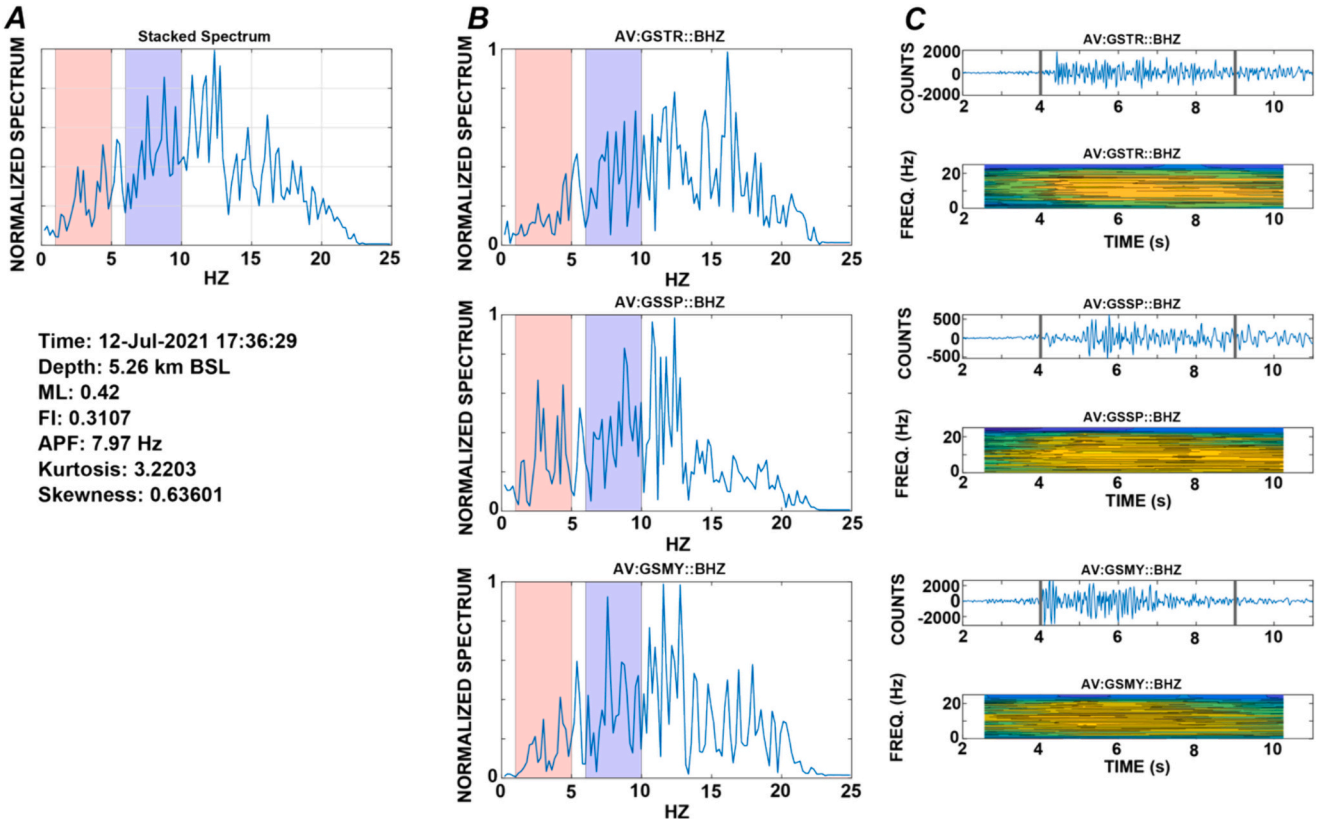


**Fig. 6.** Example of a well-classified VT earthquake. (*A*) Stacked spectrum used for classification and origin and classification metrics. Red shaded area indicates $A_{lower}$ and blue shaded area indicates $A_{upper}$. (*B*) Individual spectra for the three closest seismic stations in the Great Sitkin Volcano network. (*C*) Individual waveforms and spectrograms for the three closest stations used for auto-classification (after the taper and filter have been applied – see section 4.2). Solid lines in waveforms indicate time window used for spectra calculation. (For interpretation of the references to color in this figure legend, the reader is referred to the web version of this article.)

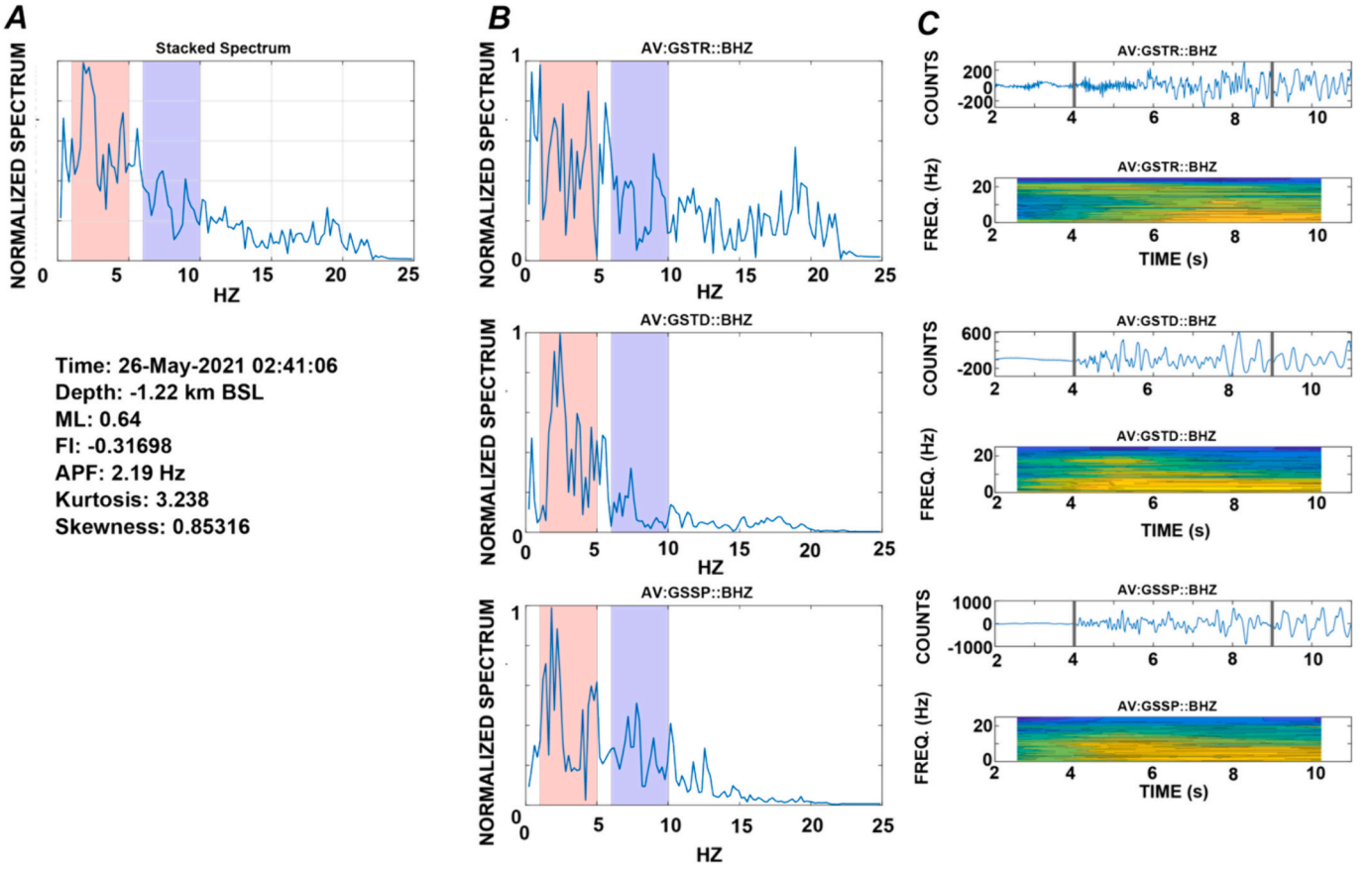


**Fig. 7.** Example of a well-classified LP event. (*A*) Stacked spectrum used for classification and origin and classification metrics. Red shaded area indicates $A_{lower}$ and blue shaded area indicates $A_{upper.}$ (*B*) Individual spectra for the three closest seismic stations in the Great Sitkin Volcano network. (*C*) Individual waveforms and spectrograms for the three closest stations used for auto-classification. Solid lines in waveforms indicate time window used for spectra calculation. (For interpretation of the references to color in this figure legend, the reader is referred to the web version of this article.)

reflect the break between VT and LP events determined by the frequency bands used in our FI calculations.

#### 4.2.1. *Autoclassification results for full dataset*

We applied the autoclassification algorithm to the full dataset of 9811 events, 9632 of which ran without errors. Results are summarized in Figs. 11 and 12: 82 % of the events are classified as VT (7860 events), 2 % are classified as LP (196 events), and the remaining 16 % (1576 events) were assigned an 'uncertain' classification. The 'uncertain' events occur almost exclusively after August 2016, and mostly after July 2019 (when a significant increase in the rate of VT seismicity began).

## 5. Results and discussion

To describe and analyze seismicity near Great Sitkin Volcano we show hypocenters in map and east-west cross sections for three time-periods (1999 to 2006, 2006 to 2016, and 2016 to 2023) that are characterized by activity on nearby crustal faults, quieter background activity, and precursory and eruptive seismicity respectively (Fig. 11) and time versus depth plots for the entire period of this study (1999 to 2023) and just the precursory and eruptive time period (2016 to 2023) (Fig. 12). For this discussion we show plots of hypocenters keyed to FI values in the text and identical figures keyed to APF values are shown in the supplementary materials.

### 5.1. *1999–2006*

Between 1999 and 2006 seismicity concentrates in three areas: 1) Under the summit of the volcano, 2) in an elongate cluster 10 to 15 km southwest of the volcano, and 3) in a second cluster 5 km southeast of the volcano, (Fig. 11A). Hypocenters under the summit during this period ranged in depth between −1.7 and 5 km and magnitude from −0.8 to 2.0 (Fig. 3). Auto-classifications indicate that these events consist of a mix of VT earthquakes and LP events (Figs. 11A and 12A) that may be indicative of shallower magmatic or hydrothermal processes that would be expected beneath the Great Sitkin Volcano summit crater. This area is coincident with the low-velocity zone identified by Pesicek et al. (2008) that is also suggestive of shallow hydrothermal and magmatic activity. During this period, we also identified a small cluster of 12 earthquakes, near Cape Akuyan (Fig. 1), just offshore of the west side of Great Sitkin Island that occur between 5 and 10 km depth.

The 2002 activity occurred as two clusters of VT earthquakes that were centered about 20 km west of the volcano at depths of −1 to 15 km in March to April of 2002 and a second cluster about 5 km southeast of the volcano between May and July 2002 at depths of 2 to 10 km. The largest earthquake in each of these clusters was a local magnitude 4.3; both M 4.3 earthquakes had strike-slip focal mechanisms that trended NE and NW (Moran et al., 2002a; see Fig. 4 in Pesicek et al., 2008). Our auto-classifications during this period show dominantly higher frequency events for the southeast cluster while hypocenters in the southwest cluster show generally lower values in FI and APF (Fig. 11A). An examination of waveforms from the SW events shows well developed P- and S-phase as expected for a tectonic rather than a volcanic sequence. It may be that the lower frequencies indicated in this area result from site or path effects that are encountered by the greater distance to the recording stations for these hypocenters or that the five second window used in our calculation was insufficient to capture the full waveform of these more distant earthquakes.

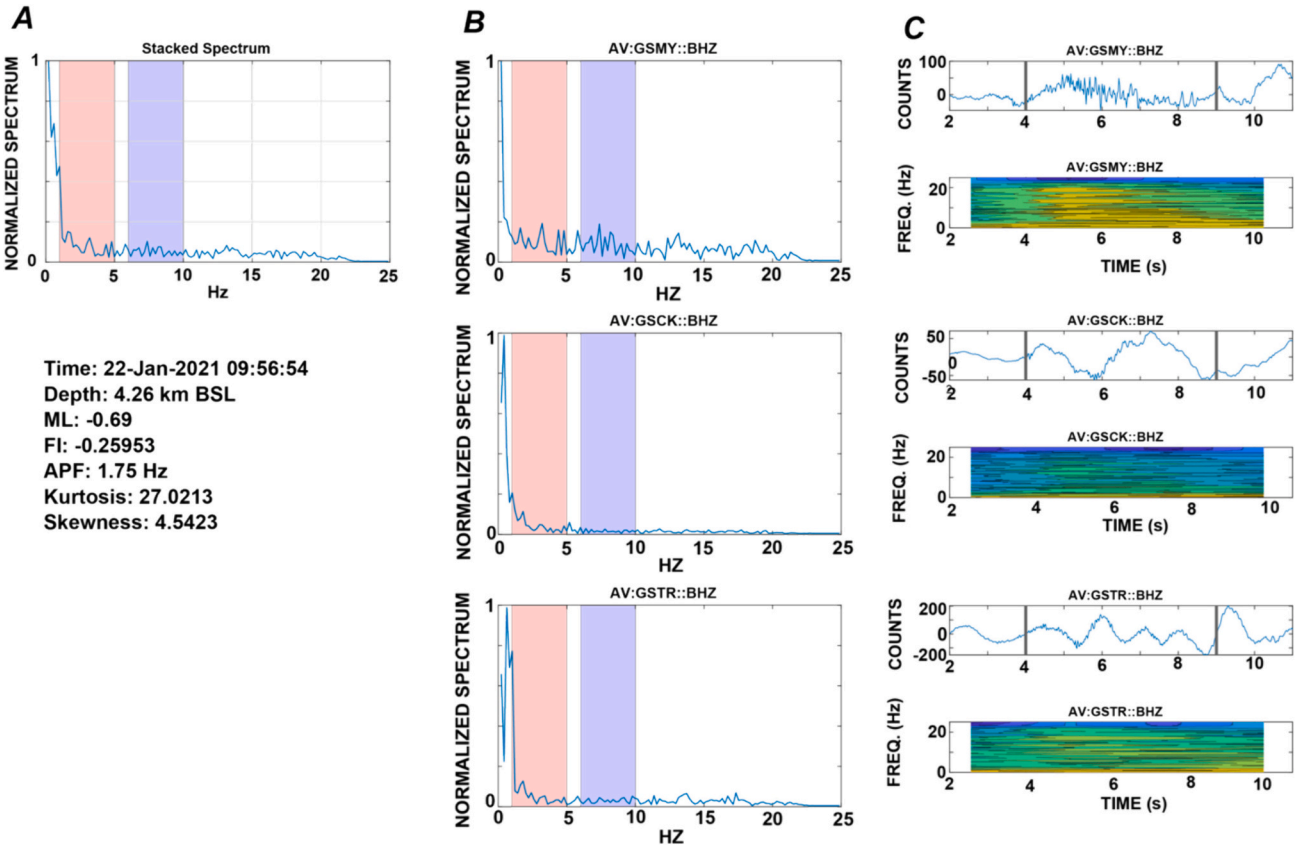


**Fig. 8.** Example of a poorly classified event. (*A*) Stacked spectrum used for classification and origin and classification metrics. Red shaded area indicates $A_{lower}$ and blue shaded area indicates $A_{upper.}$ (*B*) Individual spectra for the three closest seismic stations in the Great Sitkin Volcano network. (*C*) Individual waveforms and spectrograms for the three closest stations used for auto-classification. Solid lines in waveforms indicate time window used for spectra calculation. (For interpretation of the references to color in this figure legend, the reader is referred to the web version of this article.)

The clusters of hypocenters to the southwest and under the eastern side of the Great Sitkin edifice have been attributed to strike-slip bookshelf faulting by Ruppert et al. (2012). In contrast, Pesicek et al. (2008) attributed the SW cluster to a mainshock-aftershock sequence on a NW-SE oriented fault and the SE cluster to a dike intrusion or secondarily to a main-shock aftershock sequence. Based on the results of our auto-classification and an examination of waveforms that shows tectonic type waveforms with clear P- and S- phases in both clusters we prefer an interpretation of bookshelf faults for both clusters in 2002. Triggered or synchronous activity has been observed on adjacent bookshelf faults in Nicaragua (Cailleau et al., 2007; Higgins et al., 2022) where failure is promoted by static Coulomb stress changes on nearby or adjacent faults. Similar triggering on several adjacent bookshelf faults near the Tanaga volcanic complex, Alaska, was observed contemporaneously with a magnitude 6.6 earthquake on May 2, 2008 (Lally et al., 2023) and suggests that this process is active throughout the Andreanof Islands. Triggering by Coulomb stress changes thus seems to be the most likely cause for the earthquakes on both sides Great Sitkin Volcano in 2002 where the southeast fault activated in March and the southwest fault activated in May (Fig. 13A; see also Fig. 4 in Pesicek et al., 2008).

### 5.2. 2006–2016

Between 2005 and 2016 the volcano was relatively quiet seismically (Fig. 3). Most located events were beneath the summit at depths ranging from −1.7 to 5 km and had a mix of frequency contents similar to what was observed from 1999 through 2005. We also recorded some earthquakes with higher FI and APF values on the bookshelf faults to the southeast and southwest of the volcano indicating that these faults continued to be active during this time-period (Figs. 11B and 12A). The only notable increase in earthquake activity were two small swarms of VT earthquakes that took place on July 24 to 25 and August 28 to 30, 2013, under the volcano's summit crater. These swarms consisted of just 9 and 14 located earthquakes that ranged in depth from −1 to 2 km (Figs. 11B and 12A) and magnitude −0.6 to 0.6 (Fig. 3).

### 5.3. 2016–2023

The period from 2016 through 2022 at Great Sitkin Volcano was very active seismically as it contains the precursory sequence from July 2016 to May 2021 and the magmatic eruption from May 2021 through December 2023 (Dixon et al., 2020; Cameron et al., 2023; Orr et al., 2023; Orr et al., 2024a, 2024b). To help conceptualize the development of seismicity during this period we have plotted maps and cross sections that show the distribution of hypocenters based on ranges of FI from 2016 to 2023 (Fig. 14) and APF (Supplemental Fig. S3).

The earliest identified unrest prior to the magmatic eruption that began in May 2021 was a mix of DLP events and VT earthquakes at depths of 12 to 16 km in mid-July 2016. The first of these events was a DLP at a depth of 13 km on July 24, 2016, with an FI of −0.01 and an APF of 4.6. This was followed by a sequence of 10 identified events on July 30 with FI and APF values that ranged from −0.4 to 0.29 and 3.86 to 6.45 respectively and in magnitude from −0.8 to 0.0. While mid-crustal seismicity had been observed at Great Sitkin Volcano prior to 2016 (Power et al., 2004), a short duration increase such as this had not been detected previously (Fig. 12A). The mid-crustal events between July 24 and July 30 were shortly followed by a substantial increase in shallow LP and VT events (FI ranged from −0.34 to 0.21 and APF from 2.2 to 7.0) on July 31 (Fig. 15). Hypocenters for these shallow events clustered in depth between −1 and 2 km depth and magnitudes ranged

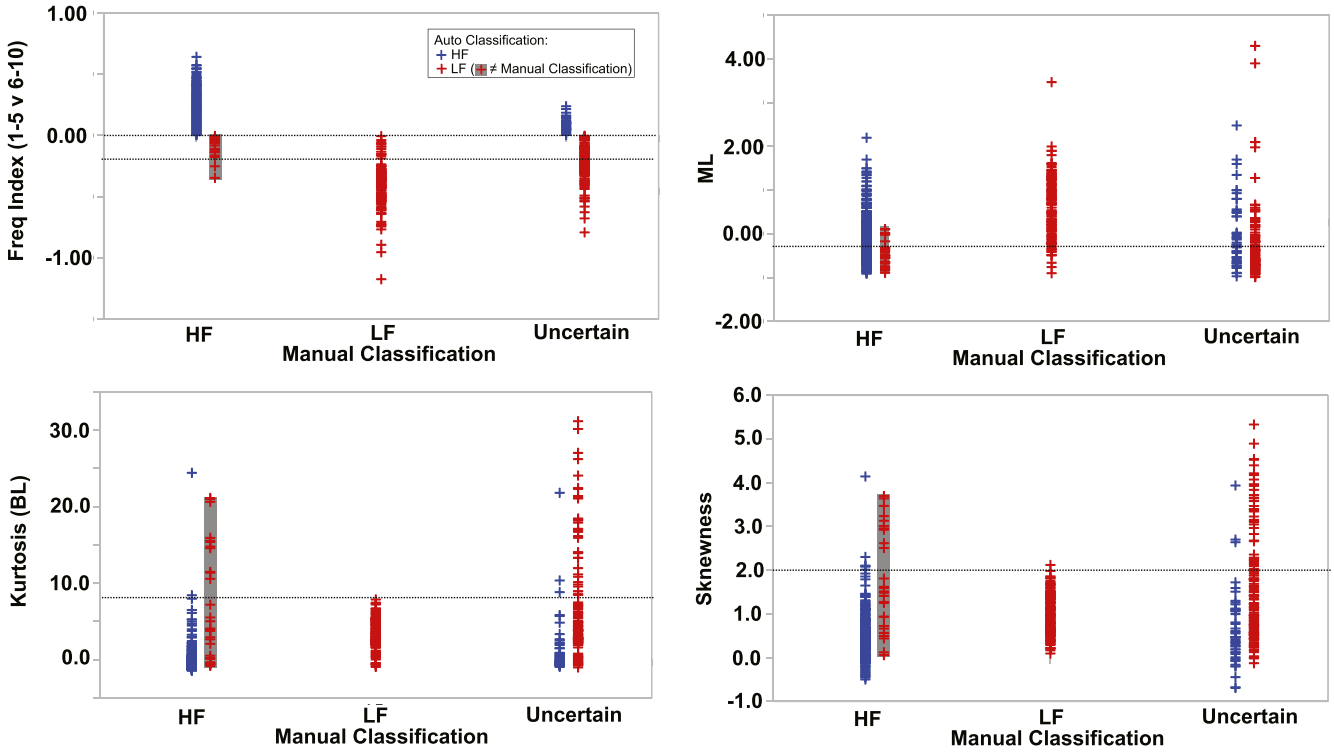


**Fig. 9.** Comparison of manual classification (X-axis) and autoclassification (color coded as in legend, gray shaded columns are incorrect autoclassifications according to manual classification) accuracy vs various parameters (Y-axes).

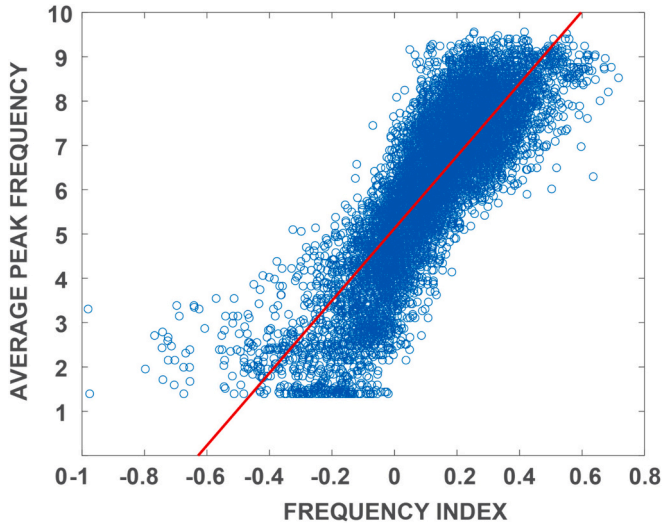


**Fig. 10.** Frequency Index (FI) plotted against Average Peak Frequency (AI). Best fit line returns an $R^2$ value of 0.84, a y-intercept of 5.13, and a slope of 8.16.

from −0.9 to −0.1. The rapid onset of shallow seismicity within 24 to 100 h of the onset of mid-crustal DLPs and VTs suggests a linkage between the mid- and upper-crust and the shallower portions of the subsurface magmatic system, although it is also possible that seismicity in these two areas was not related. The temporal history of these hypocenters implies an ascent rate of 100 to 700 m/h (Fig. 15) depending on the start time selected (First DLP on July 24 or the DLP sequence on July 30). Similar rates have been reported at Mount Pinatubo (White, 1996), Mammoth Mountain (Shelly and Hill, 2011), Kluchevskoy (Shapiro et al., 2017; Journeau et al., 2022) and elsewhere that have been attributed to pressure transients generated by degassing of volatile rich magmas at mid- to lower-crustal depths (Melnik et al., 2022). The observed increase in DLPs and VTs at mid-crustal depths in July 2016 that was rapidly followed by the onset of shallow seismicity (Fig. 15) suggests that the unrest and eruptive activity at Great Sitkin Volcano between 2016 and the present was triggered by an influx of magma in the mid-crust (10 to 20 km depth).

The shallow system at Great Sitkin Volcano then entered a long period of episodic earthquake activity, with events covering the full range in frequency, that continued until August 2021. Here we can roughly identify nine periods of heightened activity (Fig. 12B), although network and individual station outages resulted in some inconsistency in our ability to calculate hypocenters during this period (see section 3.0). These hypocenters ranged in depth from −1.7 to roughly 10 km and the most vigorous period occurred between January and November 2020 (Fig. 3 and 12B).

Between 2016 and 2022 shallow hypocenters (depth < 10 km) were initially concentrated beneath the summit of the volcano and ranged in depth from −1 to about 7 km. These events were largely VT earthquakes, although located events covered the full range in frequency content (Figs. 12B and 13B). In October 2017 AVO again began to locate VT earthquakes near Cape Akuyan (Fig. 1) on the west side of Great Sitkin Volcano and this area remained episodically active until late 2021 (Fig. 13B). In December of 2018 VT earthquakes began to appear on the east side of Great Sitkin Island. These hypocenters extended beyond the islands NE shoreline between Sulphur and Bugle Points (Figs. 13B, 14C and D). Earthquakes in this area continued episodically until mid-September 2021.

It is common to observe VT earthquakes surrounding long-dormant volcanoes that are building toward an eruption (e.g. Harlow et al.,

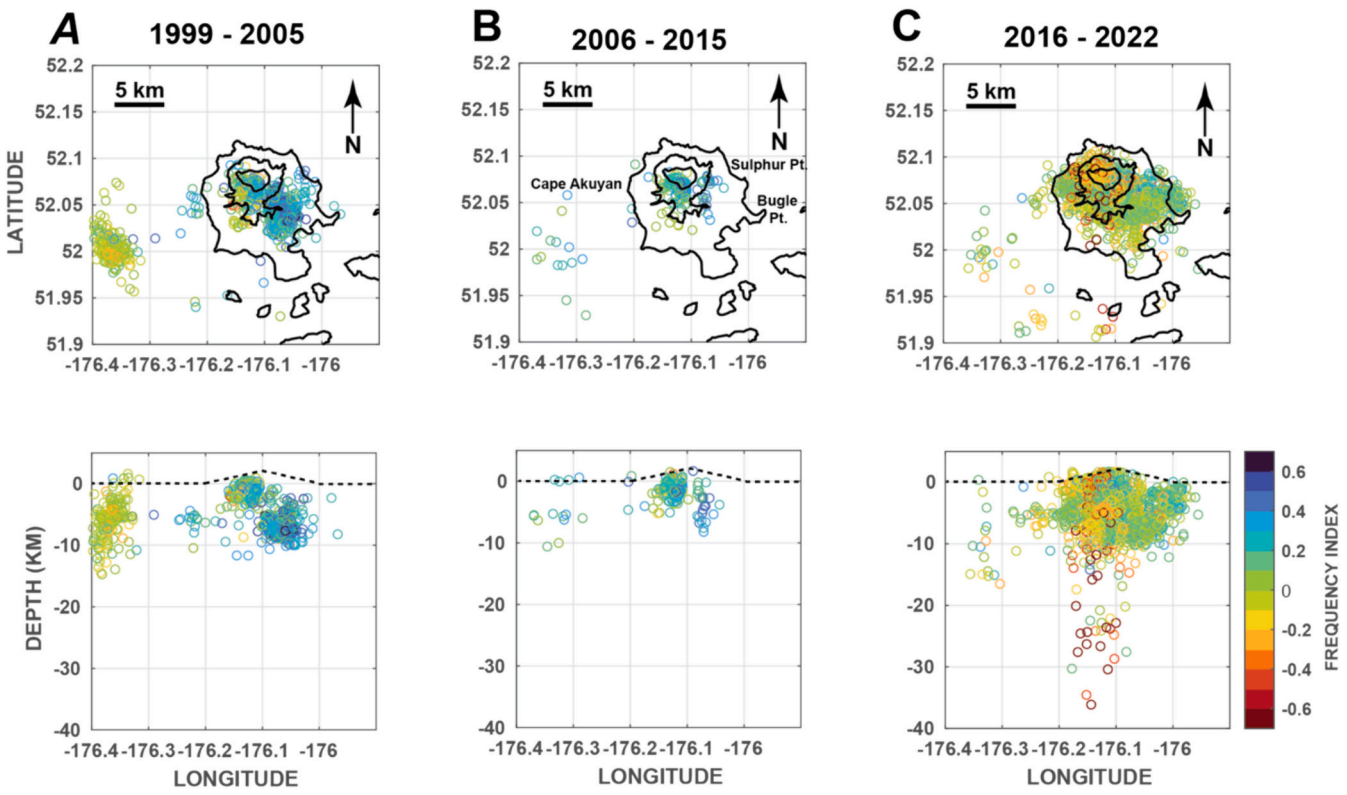


**Fig. 11.** Maps and east-west cross sections showing earthquake hypocenters near Great Sitkin Volcano for three time-periods: (A) 1999–2005, (B) 2006–2015, and (C) 2016–2022. Symbol color corresponds to the Frequency Index (FI). Black lines in maps show shorelines of Great Sitkin and neighboring islands as well as the 2000- and 4000-ft elevation contours of the Great Sitkin edifice. Dotted lines in cross sections show approximate height of topography. For a comparison with APF values see supplemental Fig. S1.

1996; Aspinall et al., 1998; Nakada et al., 1999; Moran et al., 2002b). These earthquake swarms are often attributed to changes in dynamic and static stresses, the volume and rate of magma intrusion (Roman et al., 2004) and hydrothermal fluid circulation (Shelly et al., 2013; Meyer et al., 2021). At Great Sitkin between late 2017 and late 2021 the earthquakes near Cape Akuyan and on the east side of the volcano are consistent with these processes. The VT earthquakes on the east side of the island occur over a broad area extending beyond the eastern shore of the island between Sulphur and Bugle points (Fig. 13B and 14). The earlier seismicity in 2002 on the eastern side of Great Sitkin Volcano was associated with a bookshelf fault by Ruppert et al. (2012) and Pesicek et al. (2008) suggested earthquakes in this area in 2002 were the result of either a dike injection or a fault (see section 5.2). Recently Yang et al. (2023) identified low seismic velocities on the eastern side of Great Sitkin Island and suggested this area as the site of a magma storage area that fed the ongoing eruption. Given the oblique subduction in the Andreanof Islands and the numerous bookshelf faults identified by Ruppert et al. (2012) and Lally et al. (2023), the dominantly higher FI and APF values for earthquakes located in this area (Figs. 11, 13, and 14), and the apparent stress triggering of earthquakes on adjacent faults observed near Great Sitkin in 2002, we favor an interpretation involving stress triggering similar to that developed for central America (Higgins et al., 2022) or hydrothermal fluids (Shelly et al., 2013; Meyer et al., 2021) for the earthquake activity on the east side of Great Sitkin between 2018 and 2021. The broad extent of these VT hypocenters that extend beyond the island's eastern shoreline near Sulphur and Bugle points suggest both processes may have been active in this between 2019 and 2022 (Fig. 13B and 14C). However, Cailleau et al. (2007) and Higgins et al. (2022) have also identified a temporal correlation between volcanic unrest at Momotombo Volcano in Nicaragua and triggering of earthquake activity on nearby bookshelf faults. Triggering because of stress transfer between the SE bookshelf fault may also be a possibility for earthquakes between 2018 and 2021. The area near Cape Akuyan may represent activation by changes in fluid pressure or a previously unrecognized bookshelf fault in this area.

The precursory unrest at Great Sitkin Volcano from mid-July 2016 to mid-May 2021, of more than 1760 days, is unusually long for a precursory volcano-seismic sequences. Comparative studies of precursory seismic duration by Benoit and McNutt (1996), Passarelli and Brodsky (2012), and White and McCausland (2019) identified longer runup durations that reach $2 \times 10^3$ days for volcanoes such as Mount Unzen (Nakamura, 1995) and Popocatépetl (De la Cruz-Reyna and Siebe, 1997). Passarelli and Brodsky (2012) found a positive relationship between duration of precursory unrest, higher silica contents, and eventual erupted volume. This suggests that the ongoing effusive eruption at Great Sitkin Volcano may continue for some time.

In mid- to late-July 2021 lava began to erupt in the Great Sitkin summit crater forming first a small lava dome and then flows that extended down the SE and SW sides of the volcano's edifice. The rate of lava extrusion was estimated at $7 m^3/s$ in August, dropped to $2 m^3/s$ in September, and then declined further to below 1 $m^3/s$ in November 2021 (Orr et al., 2024b). Earthquake activity largely stopped roughly coincident with the decline in effusion rates in September 2021 (Fig. 13B).

The rate of located events increased again at Great Sitkin Volcano between June and September of 2022. These hypocenters were dominantly LP events beneath the volcano's summit at depths of 5 to 12 km (Fig. 12B and 13B) and magnitudes ranged from −1.0 to 1.0 (Fig. 3). These LPs were coincident with a period of increased eruptive activity when effusion rates climbed to 1 to 2.5 $m^3/s$ (Orr et al., 2024b). These hypocenters were deeper than those observed earlier in the precursory and eruptive sequence and suggest that magma that fed the increased extrusion rates observed in mid-2022 was sourced from a deeper portion of the Great Sitkin magmatic system.

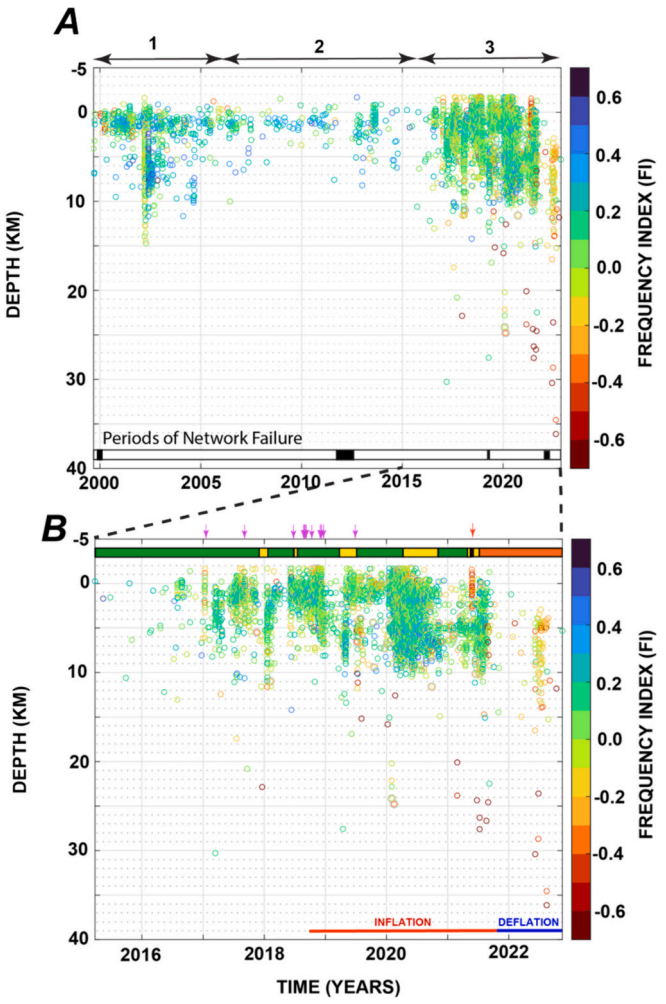


**Fig. 12.** Plots of hypocenter depth versus time for (*A*) 1999–2022 and (*B*) 2015–2022. Symbol color reflects the frequency index (FI) assigned to the individual hypocenter. The three time-periods that are characterized by activity on nearby faults (1999–2006), quieter background (2006–2016) and precursory seismicity and eruptive activity are shown along the top of *A*. Time periods when the Great Sitkin Volcano seismic network was not operational are shown as black bars at the base of *A*. Colored bar along the top of *B* reflects the aviation color code (see section 5.6) assigned to the volcano by AVO. Purple arrows show times of small presumably phreatic explosions between 2017 and 2019 and red arrow notes time of magmatic explosion on May 26, 2021. Periods of inflation and deflation identified by Wang et al. (2023) are noted along the base of *B*. For a comparison with APF values see supplemental Fig. S2. (For interpretation of the references to color in this figure legend, the reader is referred to the web version of this article.)

Seismicity in the mid- to lower-crust (10 to 40 km) also slowly increased between 2016 and 2022 with progressively more DLP events identified. The network upgrade to three-component digital broadband seismometers in 2019 may be responsible for some of the increased observation rate, however the initial increase began in 2016 well ahead of the improvements in instrumentation (see section 3.0). The rate of DLP event detection reached apparent maxima shortly after the May 26, 2021, explosion and then again in mid-2022 apparently in association with the observed increase in magma extrusion rate (Orr et al., 2024C). Hypocenters for many of these DLP events were located in the lower-crust at depths of 20 to 40 km (Fig. 12B).

### 5.4. Explosive activity: 2017–2021

On January 11, 2017, AVO identified what was the first of a series of 15 small explosive events that took place between January 2017 and June 2019. Typically, these events began impulsively, had extended codas, and peak frequencies below 5 Hz. The larger explosion events typically were followed by increased VT and LP events activity that exhibited FI and APF values of −0.05 to 0.5 and 0.42 to 8.5 and continued for tens of minutes to as much as 24-h. Fig. 16 shows 24-h Helicorder style records of the waveforms from station GSSP for the larger explosive events. To quantify the size of the explosions at Great Sitkin Volcano we measured the duration of the seismic signal at station GSSP from the time that signal first exceeded twice the seismic background to the time the signal returned to this level in a method identical to that used by Searcy and Power (2020). Table 2 contains the duration measurements and Fig. 16F shows the progression of explosion events between 2016 and 2022. The explosion at 00:17 UTC on July 22, 2017, had the longest duration of 80.7 min. As a result of lack of consistent visual observation of the volcano's summit crater some ambiguity exists as to whether shorter duration signals (typically those less than about 2 min) reflect actual explosions or short episodes of volcanic tremor.

The only confirmation that these seismic signals correspond to explosions comes from the event on June 10, 2018, that produced an ash deposit that was clearly visible in satellite imagery on the snow and extended from the summit crater to the southeast (Fig. 2C). None of the small explosion events generated infrasound signals that could be detected with instruments located in Adak (Dixon et al., 2019; Orr et al., 2024a, 2024b). Based on the similarity in waveforms and visual observations of increased steaming from the summit crater (Fig. 2B) we suggest that all these events represent small phreatic, or water/steam driven explosions. Because of the remote location of Great Sitkin Volcano no samples of any deposits from these explosions were ever collected. (See Fig. 2)

In a recent compilation study Stix and de Moor (2018) proposed two mechanisms for phreatic eruptions that precede magmatic activity: Type 1, where magmatic fluids are injected into a sealed hydrothermal system until over-pressurization ruptures the seal producing ballistics and fine ash and Type 2, wherein magmatic fluids enter a near surface hydrothermal system vaporizing liquid water generating wet ash, lahars, and ballistics. Given our limited observations of the explosions between 2017 and 2019 it seems that the Type 1 mechanism is more consistent for explosions at Great Sitkin Volcano. All these explosions followed the increase in mid- to lower-crustal events that began in July 2016 and the onset of increased seismicity at depths of −1 to 10 km beneath the summit crater (Figs. 12B and 15). With this observed seismic activity we would expect magmatic fluids to be rising and likely accumulating beneath barriers perhaps associated with the lava dome that was emplaced at the end of the 1974 eruption.

The explosion on May 26 at 05:03 UTC differs markedly in character from the earlier explosions sending a plume of ash and gas to an altitude of 15,000 ft. above sea level and producing a strong infrasonic signal in Adak (Fig. 2D). Eruptive products from this explosion were collected in the summer of 2021 and were found to contain rare juvenile breadcrust bombs with a bulk andesite composition and a rhyolite matrix glass confirming the involvement of fresh magma. Analysis of these rocks suggests that the magmatic phase of the eruption was triggered when fresh magma from depth blasted through a colder plug of old magma or lava (Orr et al., 2024b).

Unlike earlier explosions in 2017 through 2019 this explosion was preceded by roughly two weeks of slowly increasing seismicity, increased temperatures in the summit area observed in satellite imagery (Orr et al., 2024b), and 24 h of precursory LP events with FI and APF values that ranged from −0.6 to −0.2 and 1.6 to 4.0 respectively (Fig. 17). The waveforms from these LP events had impulsive P-arrivals and poorly developed indistinct S-waves (Fig. 17B). These waveform characteristics made it very difficult to determine accurate hypocenters

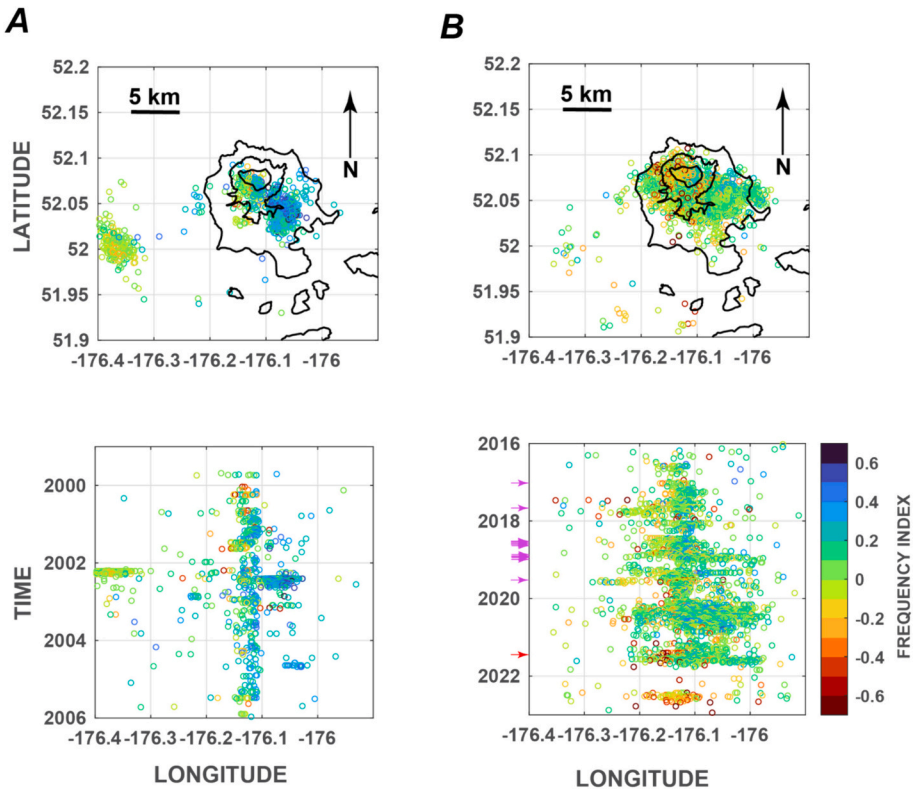


**Fig. 13.** Epicenter maps and longitude versus time for (*A*) 1999 to 2006 and (*B*) 2016 to 2023. Symbols correspond to frequency Index (FI) of located events. Black lines in maps correspond to shorelines of Great Sitkin Island and surrounding islands and 2000- and 4000-ft elevation contours. Purple arrows along the time axis in (*B*) indicate the occurrence of explosions between 2017 and 2019 and red arrow indicates the magmatic explosion on May 26, 2021. (For interpretation of the references to color in this figure legend, the reader is referred to the web version of this article.)

using the standard techniques and metrics required for inclusion in the AVO earthquake catalog (Dixon et al., 2019). To locate these LP events more accurately, we recovered waveform data and determined P-arrivals from the GSTD digitizer where telemetry had failed (October 2020 to June 2022). We then relocated the 163 hypocenters from the AVO catalog in the 48-h period prior to the May 26 explosion using only p-arrivals from the six stations closest to Great Sitkin Volcano (Fig. 1). This reduced the average horizontal and vertical errors, RMS, and GAP from 1.28 km, 1.43 km, 0.22, and 272 degrees to 1.05 km, 0.05 km, 0.05, and 116.4 degrees respectively. The resultant hypocenters cluster very tightly between −1 and 2 km depth beneath the summit crater (Fig. 17C). These relocated LP (Fig. 17C) events on May 24–26 suggest this new magma accumulated at roughly sea level before pressurizing and explosively opening a passageway through the 1974 dome material.

Yang et al. (2023) suggested the initial explosive eruption on May 21, 2021, was fed by a magma chamber to the northwest of the volcano's summit based on a low S-wave velocity zone in this area and the original LP hypocenters on May 26 and 27 that were mis-located with poorly determined S-phases. Our relocations of these LP events (Fig. 17C) suggest this interpretation is now untenable and that this explosive eruption was more likely fed by magma from upper-crustal depths directly beneath the summit crater.

### 5.5. Magmatic system geometry, activation, and tectonic setting

Based on the spatial and temporal development of earthquake hypocenters between 1999 and 2023, the automated event classifications developed here, modeling results of deformation determined by InSAR (Wang et al., 2023) and the observations of unrest and eruptive activity we suggest that the subsurface magmatic system at Great Sitkin Volcano is comprised of the following components:

- A deeper magmatic source zone at mid- to lower-crustal depths (12–36 km) that is characterized by DLP and VT earthquakes.
- An upper-crustal magma storage area that lies between −1 and 10 km depth beneath the volcano's summit crater that is the source of shallow LPs and VTs observed between 1999 and 2023.
- A shallow seal at −1.0 to 1. km depth that is defined by the LP hypocenters on May 25 and 26, 2021 immediately prior to the major magmatic explosion.
- The Great Sitkin Volcano edifice is bounded by bookshelf faults that strike roughly NW-SE and are located roughly 15 km SW and 5 km SE of the volcano's summit.

Based on the spatial and temporal development of seismicity we believe the 2021 to present (June 2024) magmatic eruption was initiated by a deeper intrusion of magma marked by the occurrence of DLP and VTs at mid- to lower-crustal depths starting in mid-July 2016. The onset of DLP and VT earthquakes at mid-crustal depths in late-July 2016 was followed almost immediately by VT and LP events at depths of −1.0 to 2.0 km depth that presumably marked the rise of magmatic volatiles or pressure transients from the mid-crust to near sea level (Fig. 15). This set off the episodic sequence of seismic events that contained a mix of frequencies between 2017 and 2023 that principally clustered beneath the summit at depths of −1 to 10 km depth (Fig. 12). We attribute this seismicity to a further pressurization of the upper crustal magma storage area between mid-2016 and mid-2021. This shallow (−1 to 10 km) seismicity is largely coincident with the observed inflation in InSAR data and modeled Mogi Source at 5 to 7 km depth (Wang et al., 2023).

Starting in late 2017 the increasing shallow stress and increasing fluid pressures activated the bookshelf fault and surrounding areas east of the Great Sitkin edifice extending beyond the island's eastern shoreline (Fig. 14). The increasing presence of magmatic fluids beneath the summit crater caused increased heat flux, observations of increased

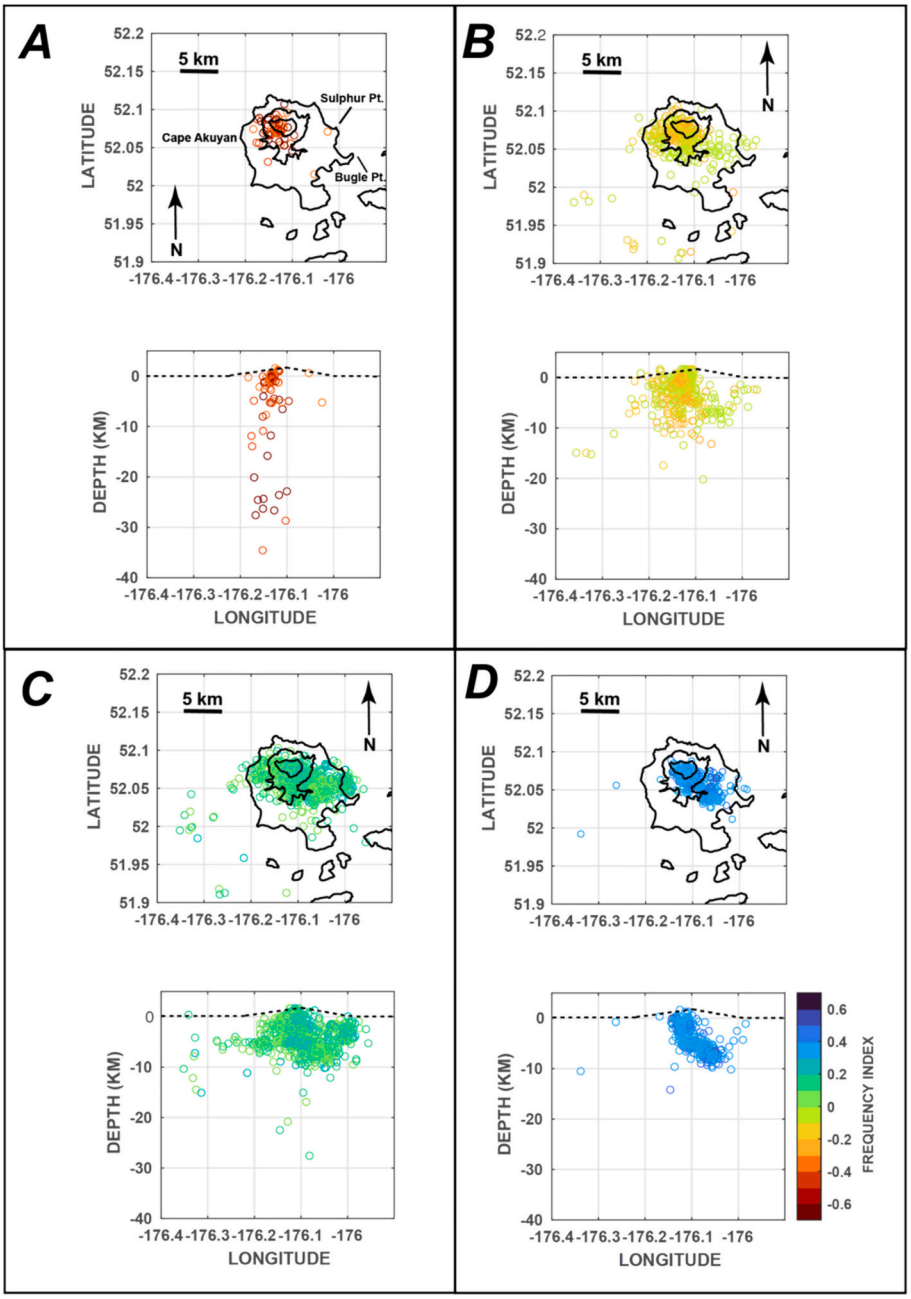


**Fig. 14.** Maps and east-west cross sections showing earthquake hypocenters from 2016 to 2023. Symbol color reflects calculated FI values of FI with (*A*) -0.8 to −0.39, (*B*) -0.4 to 0.99, (*C*) 0.0 to 0.39, (*D*) 0.4 to 0.8. Black lines in map view correspond to shorelines of Great Sitkin and adjacent islands as well as 2000- and 4000-ft elevation contours on Great Sitkin Island. Dotted lines in cross sections show approximate elevation of topography. For a comparison with APF values see supplemental Fig. S3.

steaming in late 2017 (Fig. 2B), and generated the small, presumably phreatic, explosions between January 2017 and June 2019 (Fig. 16). Eventually this pressurization culminated in the 24-h long sequence of shallow LP events (Fig. 17) that immediately preceded the magmatic explosion on May 26, 2021 (Orr et al., 2024b). Both shallow swarms of VTs and LPs on July 30, 2016 (Fig. 15) and May 25–26, 2021 (Fig. 17) occurred in remarkably similar locations and depth. We think these hypocenters likely mark the position of a cap or seal on the upper-crustal storage area that is perhaps the base of the lava dome emplaced at the end of the 1974 eruption (Fig. 18). The events on May 25 and 26 presumably mark the destruction of this cap that led to the magmatic explosion on May 26, 2021 (Fig. 17). This explosion opened a pathway for magma to move to the summit crater forming a lava dome and subsequent flows that began to form in late July 2021. Shallow VT and LP events continued until mid-September when lava effusion accelerated (Orr et al., 2024b) and the Great Sitkin edifice began to subside (Wang et al., 2023). This presumably marks a further opening of the pathway to the surface so that the movement of magma no longer stressed the volcanic edifice or surrounding shallow crust (Fig. 13B).

Between June and August 2022 AVO again located a mix of LP and VT events under the summit that generally ranged in depth between 3 and 15 km and in magnitude between −0.5 to 0.7. This seismicity is associated with an increase in eruptive rate to 1 to 2.5 $m^3/s$ observed in satellite imagery (Orr et al., 2024C) and the ongoing subsidence of the edifice identified by Wang et al. (2023). The greater depths of these LP events suggest the increased eruptive rate in the summer of 2022 may

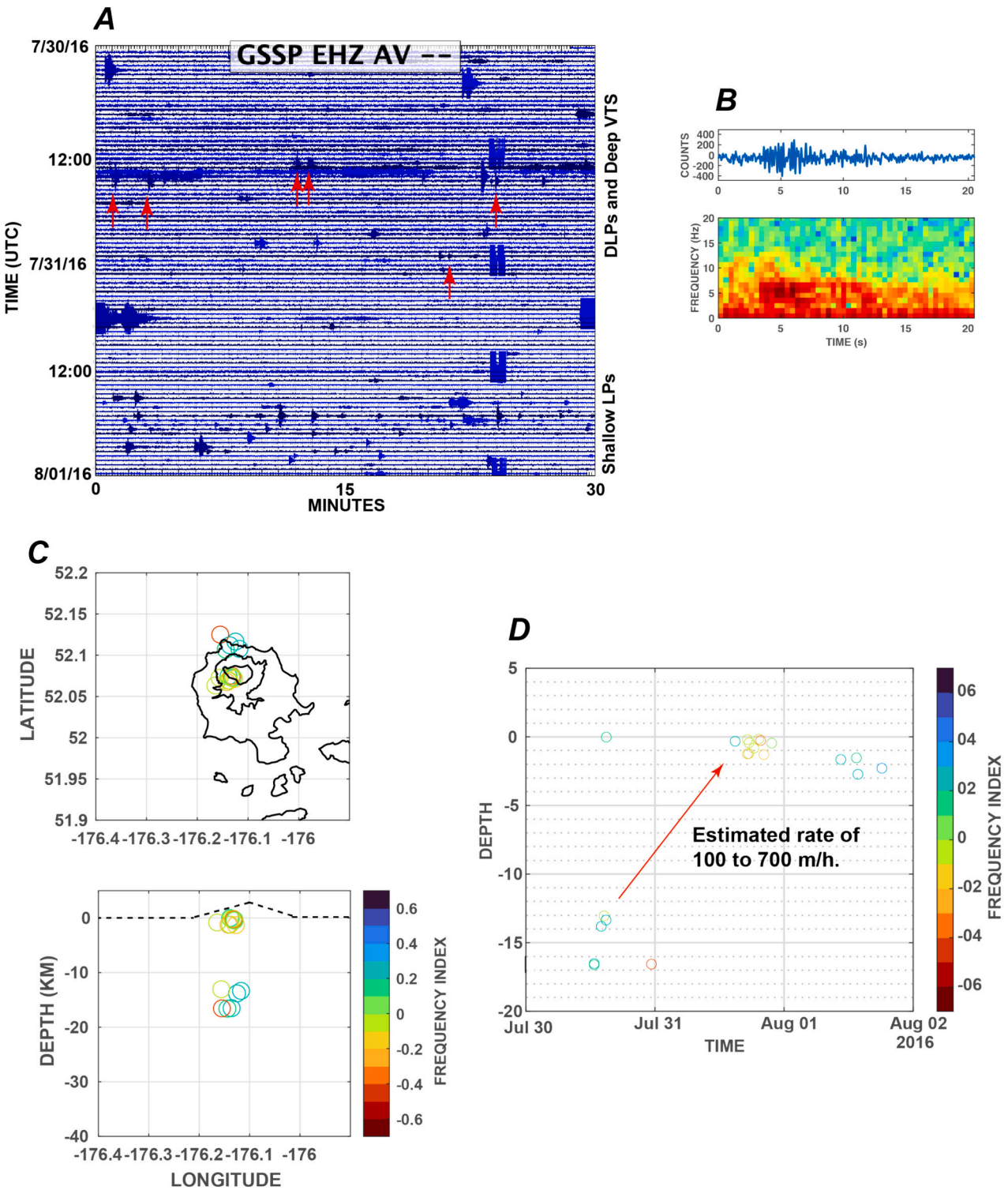


**Fig. 15.** (*A*) 48-h velocity seismic record from station GSSP that shat shows mid-crustal DLP and VT seismic events on July 30 (occurrence of located events on July 30 are noted by red arrows) and subsequent shallow swarm of VT earthquakes on July 30, 2016. (*B*) the waveform and spectrogram of a DLP event at 23:21 UTC on July 30, 2016, at a hypocentral depth of ~16 km and FI and AF values of −0.41 and 3.86 respectively. (C) Epicentral map and east-west cross section of hypocenters on July 30 and 31, 2016. Symbol color corresponds to FI value. Solid lines in map view represent shorelines of Great Sitkin Island and surrounding islands as well as 2000- and 4000-ft contours on Great Sitkin Volcano. Dotted line in cross section reflects approximate height of tomography. (*D*) Time depth plot of located events at Great Sitkin between July 30 and August 1, 2021. Calculated hypocenters suggest an upward pressure migration at rates of 100 to 700 m/h. (For interpretation of the references to color in this figure legend, the reader is referred to the web version of this article.)

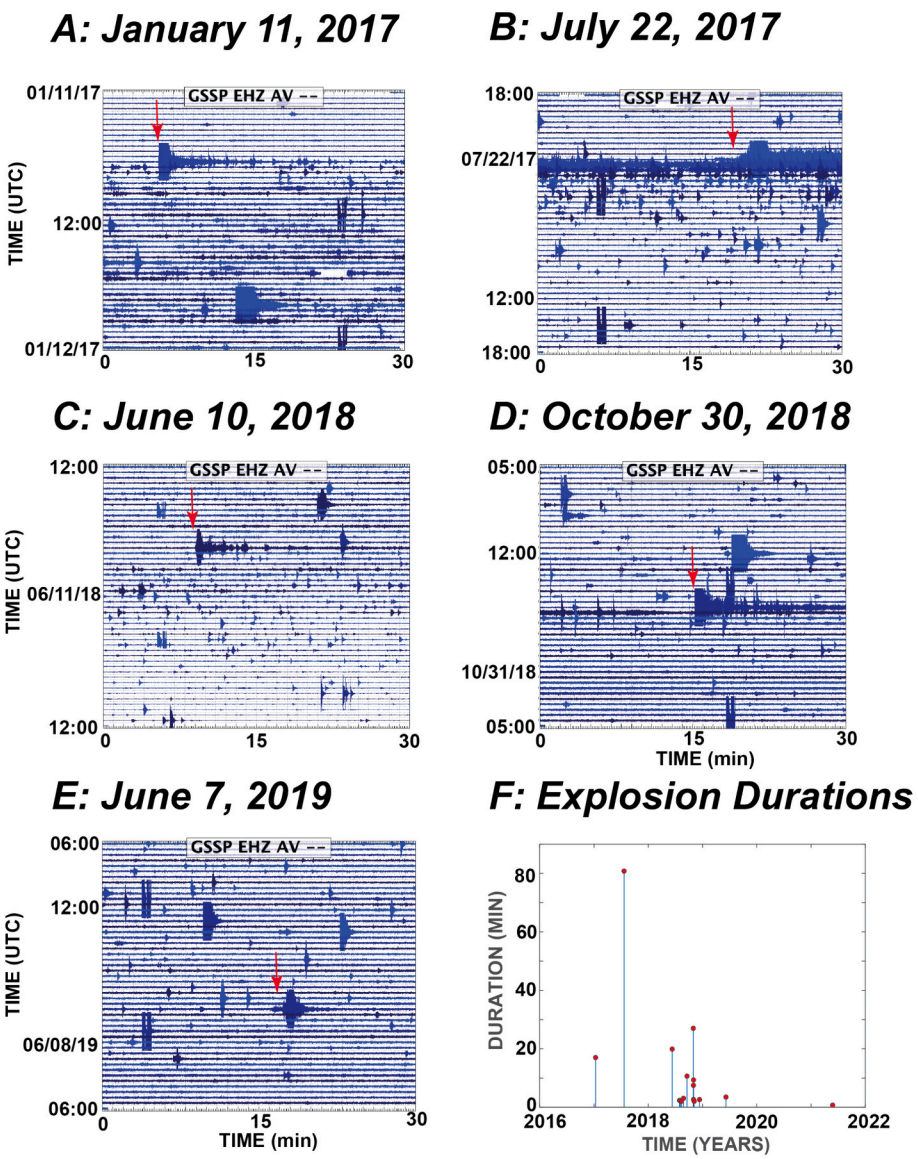


**Fig. 16.** Twenty-four-hour velocity seismic records from station GSSP for explosion signals on (*A*) January 11, 2017, (*B*), July 22, 2017, (*C*) June 10, 2018, (*D*) October 30, 2018, (*E*) June 7, 2019. Note that all of these explosions are followed by increased rates of shallow VT earthquake activity. (*F*) Durations of explosion events.

**Table 2**
Explosion time and duration (min.)

| Explosion Date and Time (UTC) | Signal Duration (Min) |
|---|---|
| 2017/01/11 06:05 | 17.0 |
| 2017/07/22 00:17 | 80.8 |
| 2018/06/10 19:38 | 19.9 |
| 2018/07/30 13:14 | 2.4 |
| 2018/08/0319:38 | 2.2 |
| 2018/08/1119:04 | 2.1 |
| 2018/08/26 03:40 | 3.1 |
| 2018/09/18 11:05 | 10.7 |
| 2018/10/30 18:15 | 27.0 |
| 201,810/31 23:39 | 7.5 |
| 2018/11/01 17:47 | 2.7 |
| 2018/11/01 17:58 | 9.4 |
| 2018/11/06 01:57 | 2.1 |
| 2018/12/11 15:04 | 2.6 |
| 2019/06/07 21:17 | 3.5 |
| 2021/05/26 05:03 | 0.8 |

have tapped a deeper portion of the magmatic system in the upper crust. DLP events during this period between 10 and 36 km were also detected (Fig. 12B) suggesting continued or additional influx of magma from the lower crust. The estimated erupted volume at the end of 2021 was 0.031 $km^3$ (Orr et al., 2024b).

### 5.6. Eruption forecasting

In this section we review the public statements and warnings that AVO issued between 2016 and 2023 for Great Sitkin Volcano. The sequence of unrest and eruptive activity at Great Sitkin provides a valuable case study to evaluate the effectiveness of a long-term monitoring program at a remote andesitic volcano as it ended a roughly 43-year period of repose since the prior eruption in 1974 (Waythomas et al., 2003). Eruption forecasts are most effective when multiple data streams such as seismicity, ground deformation, gas flux, are analyzed concurrently in conjunction with knowledge of past eruptive behavior, visual observations of the volcano, and other signs of unrest. At AVO the general strategy is to consider as many disparate information sources as possible when formulating forecasts, however, the remote setting of

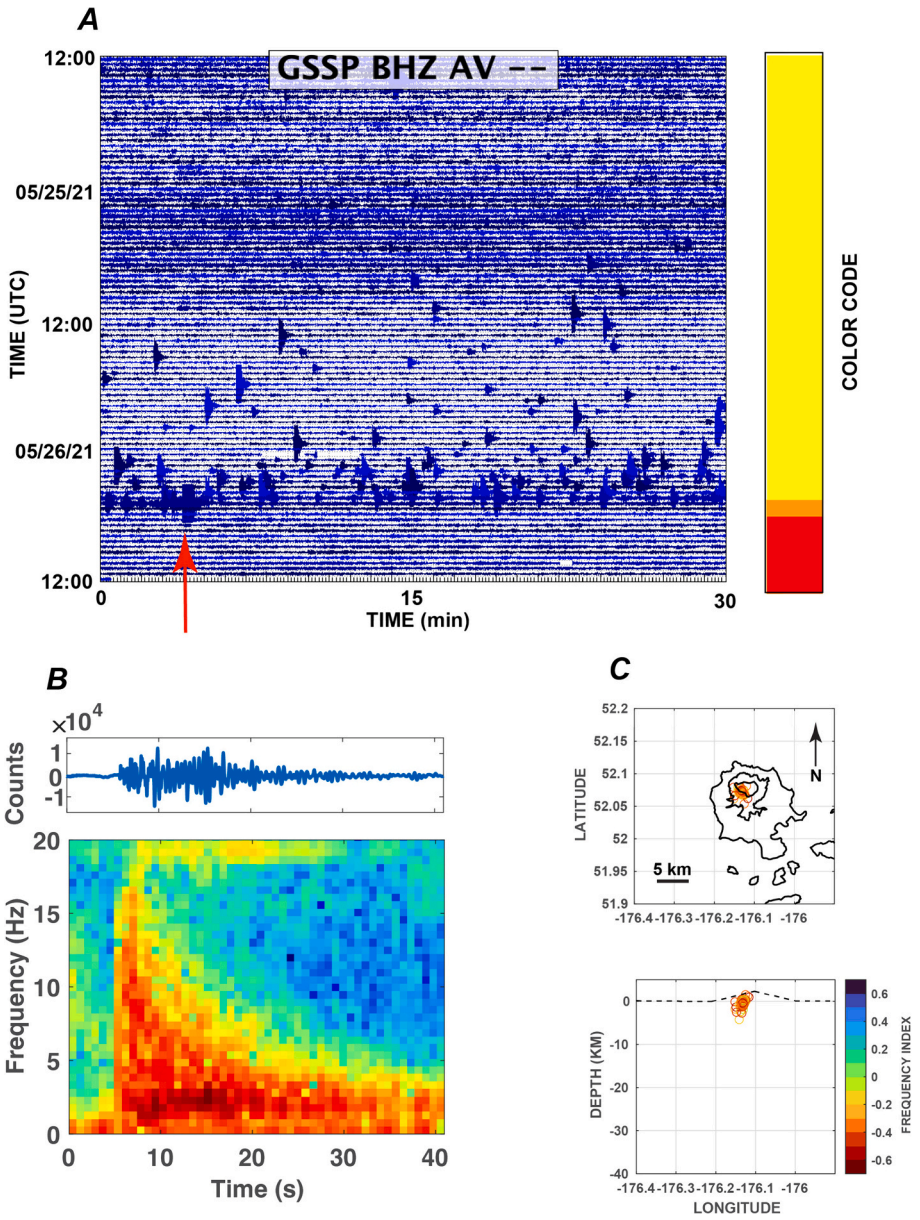


**Fig. 17.** (A) Forty-eight-hour velocity seismic record from station GSSP showing the shallow (−1 to 2 km depth) LP swarm that immediately proceeded the May 26, 2021, explosion. Red arrow notes time of explosion at 05:03 UTC and bar on right reflects the color codes (see section 5.6) used by AVO to warn of the impending eruption. (B), Waveform and spectrogram of a LP event on May 26 at 04:48 UTC, and (C), map and cross-section of LP hypocenters located using only P-arrivals on May 25 and 26, 2021. Symbol color corresponds to the frequency index (FI). Black lines in map correspond to coastline and 2000- and 4000-ft contours on Great Sitkin Island. Dotted line represents approximate elevation of topography in cross section. (For interpretation of the references to color in this figure legend, the reader is referred to the web version of this article.)

many volcanoes in Alaska and persistent storms and cloud cover in the Aleutians often limits some of these observations.

The AVO issues public notices of volcanic unrest and eruption using a dual warning system designed to communicate both ground-based hazards that has four advisory levels and a four-tiered color-coded system to communicate hazards for aircraft (Gardner and Guffanti, 2006). The color codes and alert levels are raised or lowered in response to changes in volcanic unrest and observations of eruptive activity. Immediate warnings are communicated by telephone call down to affected government agencies such as the Federal Aviation Administration, National Weather Service, and the Alaska Division of Homeland Security and Emergency Management. These immediate warnings are followed by several written forms of communication that include Volcanic Activity Notice (VAN), Volcano Notice for Aviation (VONA), Status Reports, and Information Statements. Details on the use and dissemination of these notifications at AVO are reviewed by Neal et al. (2010) and Coombs et al. (2018). The public notices of changing unrest and eruption issued in response to observed unrest at Great Sitkin Volcano between 2016 and 2022 are summarized in Table 3 as well as graphically in Figs. 12 and 17. In the following discussion we will focus on the changes to aviation color code as Great Sitkin island has no permanent residents and the principal hazards from eruptions at Great Sitkin Volcano are to overflying aircraft.

The first public notice of unrest at Great Sitkin Volcano was a status report on July 22, 2017, that followed the extended seismic signal associated with the explosion on July 22, 2017 (Fig. 16B and F). This was followed by an Information Statement on July 26 that described earlier unrest including the increase in seismicity starting in July 2016 and the explosion on January 11, 2017. AVO first raised the color code on November 22, 2017, when increased steaming of the volcano was

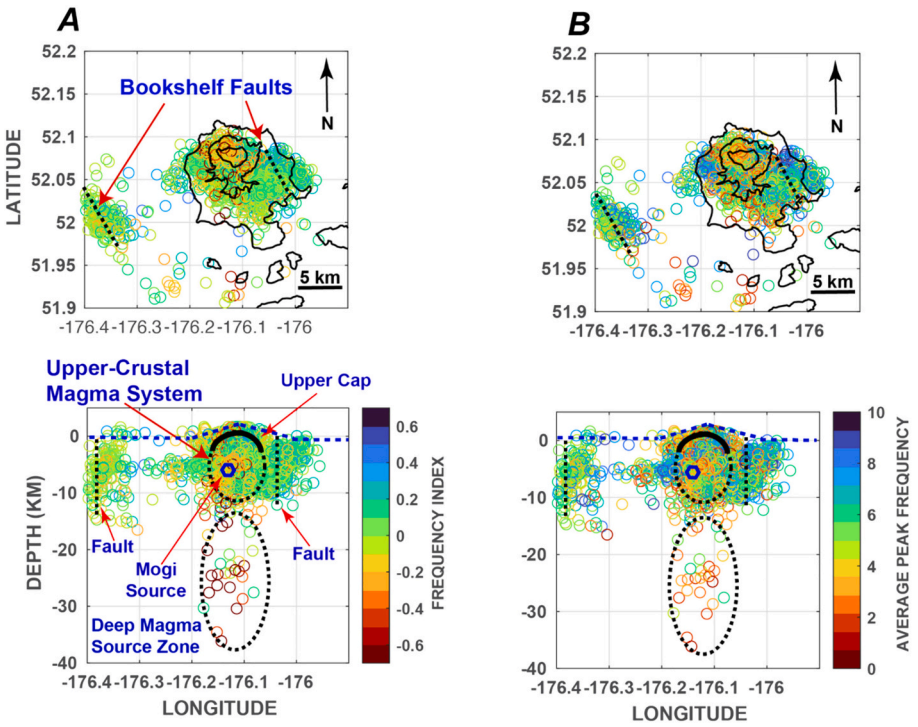


**Fig. 18.** Conceptual model of the Great Sitkin Volcano magmatic system overlain on earthquake hypocenters from 1999 to 2023 where symbol color reflects the frequency index (A) and average peak frequency (B). Black dashed lines in cross section note the approximate extent of mid- to lower-crustal magma source area and upper-crustal magma storage areas. Black dotted lines in map and cross section are inferred location of bookshelf faults. Solid black lines in map reflect coastline of Great Sitkin Island and surrounding islands as well as the 2000- and 4000-ft elevation lines on Great Sitkin Volcano. Dotted pink line in cross section notes approximate elevation along cross section. Blue hexagon notes the approximate location of the Mogi Source identified in InSAR data by Wang et al. (2023). (For interpretation of the references to color in this figure legend, the reader is referred to the web version of this article.)

observed from Adak in combination with the ongoing increased seismicity. The long episodic precursory seismic sequence between mid-2016 and mid-2021 proved to be a challenging sequence for eruption forecasting. AVO changed the color code between Green and Yellow 11 times and issued two Information Statements and one Status Report during this almost five-year period (Table 3).

Another particularly challenging sequence of events for eruption forecasting where the small presumably phreatic explosions that occurred between January 11, 2017 and June 7, 2019 (Table 2, Fig. 16). Forecasting phreatic explosions in the short-term is very challenging as they often lack easily identifiable precursors (Roman et al., 2016; Stix and de Moor, 2018; Jolly et al., 2010; Mannen et al., 2019, and references therein). None of these apparent small explosions had easily identifiable precursors that were apparent in seismic data in the hours to days before their occurrence. However, the seismic network at Great Sitkin Volcano only had short-period analog instruments while these explosions were taking place (Dixon et al., 2019). Consequently, AVO only made public announcements of their occurrence after the fact.

While short-term forecasting of these explosions was not possible, the first explosion on January 11, 2017, followed the onset of mid-crustal seismicity in July of 2016 by about six months. DLP events have been tied to lower- and mid-crustal magmatic activity that has culminated in magmatic eruptions at many volcanoes including Izu-Oshima (Ukawa and Ohtake, 1987), Pinatubo (White, 1996), Shishaldin Volcano (Rasmussen et al., 2018), Redoubt Volcano (Power et al., 2013) and Klyuchevskoy (Shapiro et al., 2017). Such magmatic eruptions are often proceeded by phreatic explosions and the sequence of events at Great Sitkin Volcano suggests that close monitoring of seismicity in the mid- to lower-crust might be used to anticipate phreatic explosions on longer-time scales (weeks to months).

In contrast the larger magmatic eruption on May 26, 2021, was preceded by several weeks of increasing earthquake activity, increased surface temperature, and $SO_2$ emissions observed by satellite (Orr et al., 2024b). In response AVO raised the color code to Yellow on May 13 a full 13 days in advance of the major magmatic explosion. The explosion had a clear 24-h increase in shallow LP events that clustered in depth between −1 and 2 km directly beneath the summit crater (Fig. 17). Based on this escalating seismicity (Fig. 17) AVO raised the color code to Orange at 03:43 UTC just 80 min before the explosion's onset at 05:03 UTC. The color code was raised to Red at 05:30 once geophysical data and reports from observers confirmed the ash plume had reached substantial altitude (Fig. 2D) (Orr et al., 2024b). The color code was subsequently lowered to Orange at 16:31 UTC on May 26 and yellow on May 27 at 20:58 UTC as seismicity declined.

The color code was returned to Orange at 22:52 UTC on July 23, 2021, when satellite imagery showed that an effusive eruption had begun (Orr et al., 2024b). The color code has remained at Orange since 2021 as the effusion of lava has continued to the time of writing (August 2024).

## 6. Summary and conclusions

Our analysis of seismicity at Great Sitkin Volcano between 1999 and 2023 lead us to the following observations and conclusions:

- Both frequency index (FI) and average peak frequency (APF) provide an accurate and consistent measure of the frequency content of located seismic events given the network configuration and distribution of hypocenters near Great Sitkin Volcano between 1999 and 2023.
- The classification and progression of hypocenters suggests the subsurface Great Sitkin Volcano magmatic system consists of a mid- to lower- crustal source zone between 10 and 40 km depth and an upper crustal magma storage area between −1 and 10 km depth. The upper

**Table 3**
Summary of public warnings at Great Sitkin Volcano, 1999–2022.

| Date | Time (UTC) | Color code or statement | Observation |
|---|---|---|---|
| 2017/07/22 | | Status Report | Notice of July 22 Explosion |
| 2017/07/26 | 01:19 | Info. Statement | Increased Seismicity + review of 2016 and 2017 unrest |
| 2017/11/22 | 19:57 | YELLOW | Increasing seismicity and steam |
| 2018/01/18 | 22:36 | GREEN | Decreasing earthquake activity |
| 2018/06/10 | 21:26 | YELLOW | Increasing earthquake activity and small explosion at 19:39 UTC |
| 2018/06/27 | 18:49 | GREEN | Declining earthquake activity |
| 2018/07/01 | 18:37 | YELLOW | Increasing earthquake activity |
| 2019/02/25 | 20:30 | GREEN | Declining earthquake activity |
| 201,906/02 | 19:30 | YELLOW | Explosion at 05:40 UTC |
| 2019/07/15 | 1939 | GREEN | Declining earthquake activity |
| 2020/02/26 | 20:58 | YELLOW | Increasing earthquake activity |
| 2020/03/06 | 21:24 | Info Statement | Magnitude 3.5 earthquake at 15:31 03/03/2020 |
| 2020/10/21 | 23:21 | GREEN | Declining earthquake activity |
| 2021/05/13 | 00:57 | YELLOW | Increase in surface temperatures in summit crater, gas emission, and earthquake activity. |
| 2021/05/26 | 03:43 | ORANGE | Increasing earthquake activity |
| 2021/05/26 | 05:30 | RED | Explosion at 05:04 UTC |
| 2021/05/27 | 16:31 | ORANGE | Declining seismicity |
| 2021/05/27 | 20:58 | YELLOW | Declining seismicity |
| 2021/07/23 | 22:25 | ORANGE | Circular area of uplift observed in summit crater |
| 2021/09/10 | 20:51 | Info. Statement | Lava extrusion in summit crater |

crustal area was likely capped by the 1974 lava dome until the magmatic explosion on May 26, 2021.

- Precursory seismic unrest for the 2021-present magmatic eruption began with a sequence of mid-crustal deep-long-perid (DLP) and volcano-tectonic (VT) earthquakes at depths of 13–16 km in July 2016, that was immediately followed by an increase in shallow LPs and VTs at depths of −1.0 to 1.0 km depth suggesting a linkage between the deeper and shallow portions of the magmatic system. This sequence suggests the ongoing eruption at Great Sitkin Volcano was triggered by an intrusion of magma at mid-crustal depths in July of 2016.
- Precursory unrest at Great Sitkin Volcano occurred for almost five years (July 2016 to May 2021) which is unusually long for a strato-volcano.
- Precursory unrest included a series of 15 small explosions that we presume were phreatic between January 11, 2017, and June 7, 2019.
- The magmatic explosion of May 26, 2021, was preceded by roughly 14 days of increasing seismic activity and observations of increasing temperatures and SO2 emissions detected by satellite and a prominent 24-h long swarm of LP events that locate beneath the summit crater at −1 to 2 km depth.
- The Great Sitkin edifice is surrounded by bookshelf faults that were active in 2002 and coincident activity on these faults in March and April suggests triggered activity in response to stress changes. Magmatic activity may have activated the fault on the east side of the edifice between 2019 and 2021.
- Alaska Volcano Observatory (AVO) successfully forecast the explosive onset of magmatic activity at Great Sitkin with written statements issued 13 days and 80 min prior to the May 26, 2021, explosion.

Supplementary data to this article can be found online at https://doi.org/10.1016/j.jvolgeores.2024.108182.

## CRediT authorship contribution statement

**J.A. Power:** Writing – review & editing, Writing – original draft, Visualization, Investigation, Formal analysis, Data curation, Conceptualization. **D.C. Roman:** Writing – original draft, Software, Methodology, Investigation, Formal analysis, Conceptualization.

## Declaration of competing interest

The authors declare the following financial interests/personal relationships which may be considered as potential competing interests:

John Power reports writing assistance was provided by US Geological Survey. If there are other authors, they declare that they have no known competing financial interests or personal relationships that could have appeared to influence the work reported in this paper.

## Data availability

Information for the permanent stations can be found at www.iris.mda.edu/AV. Continuous seismic data from 1999 to 2023 are archived at the EarthScope Data Management Center in Seattle, Washington. Event detected seismic data from Great Sitkin Volcano are archived at the Alaska Volcano Observatory (AVO). Hypocenter and phase data from 1999 to 2018 are available from Power et al., (2019) and since 2018 from the Advanced National Seismic System (ANSS) comprehensive catalog (ComCat): https://earthquake.usgs.gov/data/comcat/. Public statements on volcanic activity issued by the Alaska Volcano Observatory are available on the AVO website: avo.alaska.edu. The seismic event classification code developed in this manuscript is available for download at: https://github.com/dcroman/AVO_earthquake_classification. Any use of trade, firm, or product names is for descriptive purposes only and does not imply endorsement by the U.S. Government.

## Acknowledgements

We wish to thank the staff of the Alaska Volcano Observatory for much hard work assembling the seismic data from Great Sitkin Volcano between 1999 and 2003 and in response to the unrest and eruption between 2016 and 2023. The text and figures in this manuscript were improved based on comments from two anonymous reviewers and Alexandra Iezzi.

## References

Aspinall, W.P., Miller, A.D., Lynch, L.L., Latchman, J.L., Stewart, R.C., White, R.A., Power, J.A., 1998. Soufriere Hills eruption, 1995–1997: volcanic earthquake locations and fault plane solutions. Geophys. Res. Lett. 25, 3397–3400.

Benoit, J.P., McNutt, S.R., 1996. Global Volcanic Earthquake Swarm Database 1979-1989, U.S. Geol. Surv Open-file Report 96-69, p. 333.

Buurman, H., West, M.E., 2010. Seismic precursors to volcanic explosions during the 2006 eruption of Augustine Volcano. In: Newhall, C., Punongbuyan, R. (Eds.), Fire and Mud. U. of Washington Press, pp. 41–58 [In "The 2006 Eruption of Augustine Volcano, Alaska", edited by Power, J.A., Coombs. M.L., Freymueller, J.T., U.S. Geol. Surv. Prof. Paper 1769].

Cailleau, B., La Femina, P.C., Dixon, T.H., 2007. Stress accumulation between volcanoes: an explanation for intra-arc earthquakes in Nicaragua. Geophys. J. Int. 169, 1132–1138.

Cameron, C.E., Prejean, S.G., Coombs, M.L., Wallace, K.L., Power, J.A., Roman, D.C., 2018. Alaska Volcano Observatory alert and forecasting timeliness: 1989–2017. Front. Earth Sci. 6, 86.

Cameron, C.E., Orr, T.R., Dixon, J.P., Dietterich, H.R., Waythomas, C.F., Iezzi, A.M., Power, J.A., Searcy, C., Grapenthin, R., Tepp, G., Wallace, K.L., Lopez, T.M., DeGrandpre, K., Perreault, J.M., 2023. 2018 Volcanic Activity in Alaska—Summary of Events and Response of the Alaska Volcano Observatory: U.S. Geological Survey Scientific Investigations Report 2023–5029, p. 68. https://doi.org/10.3133/sir20235029.

Chouet, B.A., Matoza, R.S., 2013. A multi-decadal view of seismic methods for detecting precursors of magma movement and eruption. J. Volcanol. Geotherm. Res. 252, 108–175.

Coombs, M.L., White, S.M., Scholl, D.W., 2007. Massive edifice failure at Aleutian arc volcanoes. Earth Planet. Sci. Lett. 256, 403–418.

Coombs, M.L., Wech, A.G., Haney, M.M., Lyons, J.J., Schneider, D.J., Schwaiger, H.F., Wallace, K.L., Fee, D. Freymueller, Schaefer, J.R., Tepp, G., 2018. Short-term forecasting and destection of explosions during the 2016-2017 eruption of Bogoslof Volcano, Alaska. Front. Earth Sci. 6, 122.

De la Cruz-Reyna, S., Siebe, C., 1997. The giant Popocatepetl stirs. Nature 338, 227.

Dixon, J.P., Stihler, S.D., Power, J.A., Tytgat, G., Moran, S.C., Sánchez, J.J., Estes, S., McNutt, S.R., Paskievitch, J., 2003. Catalog of Earthquake Hypocenters at Alaska Volcanoes—January 1–December 31, 2002: U.S. Geol. Surv. Open-File Report 03–267, p. 58. https://doi.org/10.3133/ofr03267.

Dixon, J.P., Stihler, S.D., Haney, M.M., Lyons, J.J., Ketner, D.M., Mulliken, K.M., Parker, T., Power, J.A., 2019. Catalog of Earthquake Parameters and Description of Seismograph and Infrasound Stations at Alaskan Volcanoes—January 1, 2013, through December 31, 2017: U.S. Geol. Surv. Data Series 1115, p. 92. https://doi.org/10.3133/ds1115.

Dixon, J.P., Cameron, C.E., Iezzi, A.M., Power, J.A., Wallace, K., Waythomas, C.F., 2020. 2017 Volcanic activity in Alaska—Summary of Events and Response of the Alaska Volcano Observatory: U.S. Geol. Surv. Scientific Investigations Report 2020–5102, p. 61. https://doi.org/10.3133/sir20205102.

Gardner, C.A., Guffanti, M.C., 2006. U.S. Geological Survey's Alert Notification System for Volcanic Activity, U.S. Geol. Surv. Fact Sheet 2006–3139.

Geist, E.L., Childs, J.R., Scholl, D.W., 1988. The origin of summit basins of the Aleutian Ridge: implications for block rotation of an arc massif. Tectonics 7, 327–341.

Haney, M.M., Miller, D., Hotovec-Ellis, A., Thurber, C.M., Dietterich, H., 2022. Time-lapse seismic velocity changes coincident with dome emplacement at Great Sitkin volcano, Alaska. Seismol. Res. Lett. 93. N. 2B.

Harlow, D.H., Power, J.A., Laguerta, E., Ambubuyog, G., White, R.A., Hoblitt, R.P., 1996. Precursory Seismicity and forecasting of the June 15, 1991 eruption of Mount Pinatubo, Philippines. In: Newhall, C., Punongbuyan, R. (Eds.), Fire and Mud. U. of Washington Press.

Higgins, M., LaFemina, P.C., Saballos, A.J., Ouertani, S., Fischer, K.M., Geirsson, H., Strauch, W., Mattoli, G., Malservisi, R., 2022. Cascading hazards in a migrating forearc-arc system: earthquake and eruption triggering in Nicaragua. J. Geophys. Res. https://doi.org/10.1029/2022JB24899.

Jolly, A.D., Sherburn, S., Jousset, P., Kilgour, G., 2010. Eruption source processes derived from seismic and acoustic observations of the 25 September 2007 Ruapehu eruption – North Island, New Zealand. J. Volcanol. Geotherm. Res. 191, 33–45.

Journeau, C., Shapiro, N.M., Seydoux, L., Soubestre, J., Koulakov, I.Y., et al., 2022. Seismic tremor reveals active trans-crustal magmatic system beneath Kamchatka volcanoes. Sci. Adv. 8, eabj1571.

Ketner, D.M., Power, J.A., 2013. Characterization of seismic events during the 2009 eruption of Redoubt Volcano, Alaska. J. Volcanol. Geotherm. Res. 259, 45–62.

Klein, F.W., 2002. User's guide to HYPOINVERSE-2000, A Fortran Program to Solve for Earthquake Locations and Magnitudes, U.S. Geol. Surv. Open-file Report 02-171, p. 123.

La Femina, P.C., Dixon, T.H., Strauch, W., 2002. Bookshelf faulting in Nicargua. Geology 30 (8), 751.

Lahr, J.C., Chouet, B.A., Stephens, C.D., Power, J.A., Page, R.A., 1994. Earthquake classification, location, and error analysis in a volcanic environment: implications for the magmatic system of the 1989-1990 eruptions at Redoubt Volcano, Alaska. J. Volcanol. Geotherm. Res. 62, 137–151.

Lally, K.F., Caplan-Auerbach, J., Power, J.A., 2023. Volcanic and tectonic sources of seismicity near the Tanaga volcanic cluster, Alaska. Geochem. Geophys. Geosyst. 24 https://doi.org/10.1029/2023GC010891 e2023GC10891.

Lasage, P., Heap, M.J., Kushnir, A., 2018. A generic model for the shallow velocity structure of volcanoes. J. Volcanol. Geotherm. Res. 356, 114–126. https://doi.org/10.1016/j.jvolgeores2018.03.003.

Lu, Z., Dzurisin, D., 2014. InSAR Imaing of Aleutian Volcanoes, Monitoring a Volcanic Arc from Space. Springer, p. 390.

Mannen, K., Roman, D., Lenard, G., Prejean, S., Nakagawa, M., 2019. Towards forecasting phreatic eruptions: examples from Hakone Volcano and some global equivalents. EPS 71 (1), 1–6.

Melnik, O., Lyakhovsky, V., Shapiro, N.M., Galina, N., Bergal-Kuvikas, O., 2022. Deep lpong period volcanic earthquakes generated by degassing of volatile-rich basaltic magmas. Nat. Commun. 11, 3918. https://doi.org/10.1038/s41467-020-17759-4.

Meyer, K., Biggs, J., Aspinall, W., 2021. A Bayesian reassment of the relationship between seismic moment and magma intrusion volume during volcanic unrest. J. Volcanol. Geotherm. Res. 4119, 107375.

Miller, T.P., McGimsey, R.G., Richter, D.H., Riehle, D.H., Nye, C.J., Yount, M.E., Dumoulin, J.A., 1998. Catalog of Historically Active Volcanoes of Alaska, U.S. Geological Survey Open-file Report 98-0582, p. 104. https://pubs.er.usgs.gov/publication/ofr98582.

Moran, S.C., Power, J.A., Plucinski, T., Paskievitch, J.F., Dixon, J.P., 2002a. Seismicity at Great Sitkin volcano, Andreanof Islands, Alaska. EOS Trans. 83. S11C-1163.

Moran, S.C., Stihler, S.D., Power, J.A., 2002b. A tectonic earthquake sequence preceding the April–May 1999 eruption of Shishaldin Volcano, Alaska. Bull. Volcanol. 64, 520–524.

Nakada, S., Shimizu, H., Ohta, K., 1999. Overview of the 1990-1995 eruption at Unzen Volcano. J. Volcanol. Geotherm. Res. 89, 1–22.

Nakamura, M., 1995. Continuous mixing of crystal mush and replenished magma in the ongoing Unzen eruption. Geology 23 (9), 807–810.

NASEM. National Academies of Sciences, Division on Earth, Life Studies, Board on Earth Sciences, Committee on Seismology, & Committee on Improving Understanding of Volcanic Eruptions, 2017. Volcanic Eruptions and their Repose, Unrest, Precursors, and Timing. National Academies Press.

Neal, C.A., Murray, T.L., Power, J.A., Adleman, J.N., Whitmore, P.M., Osiensky, J.M., 2010. Hazard information management, interagency coordination, and impacts of the 2005–2006 eruption of Augustine volcano. In: Power, J.A., Coombs, M.C., Freymueller, J.T. (Eds.), The 2006 Eruption of Augustine Volcano, Alaska, U.S. Geol. Surv. Prof. Paper 1769, pp. 645–660 (IP-16860; 11/30/2009).

Orr, T., Cameron, C., Dietterich, H., Loewen, M., Lopez, T., Lyons, J., Nakai, J., Power, J., Searcy, C., Tepp, G., Waythomas, C., 2024a. 2020 Volcanic Activity in Alaska—Summary of Events and Response of the Alaska Volcano Observatory: U.S. Geol. Surv. Scientific Investigations Report 2024–5004, p. 34. https://doi.org/10.3133/sir20245004.

Orr, T.R., Cameron, C.E., Dietterich, H.R., Dixon, J.P., Enders, M.L., Grapenthin, R., Iezzi, A.M., Loewen, M.W., Power, J.A., Searcy, C., Tepp, G., Toney, L., Waythomas, C.F., Wech, A.G., 2023. 2019 Volcanic Activity in Alaska—Summary of Events and Response of the Alaska Volcano Observatory: U.S. Geol. Surv. Scientific Investigations Report 2023–5039, p. 64. https://doi.org/10.3133/sir20235039.

Orr, T.R., Dietterich, H.R., Fee, D., Girona, T., Grapenthin, R., Haney, M.M., Loewen, M. W., Lyons, J.J., Power, J.A., Schwaiger, H.F., Schneider, D.J., Tan, D., Toney, L., Wasser, V.K., Waythomas, C.F., 2024b. 2021 Volcanic Activity in Alaska and the Commonwealth of the Northern Mariana Islands—Summary of Events and Response of the Alaska Volcano Observatory: U.S. Geol. Surv. Scientific Investigations Report 2024–5014, p. 64. https://doi.org/10.3133/sir20245014.

Passarelli, L., Brodsky, E.E., 2012. The correlation between run-up and respose times of volcanic eruptions. Geophys. J. Int. 188, 1025–1045.

Pesicek, J.D., Thurber, C.H., DeShon, H.R., Prejean, S.G., Zhang, H., 2008. Three-dimensional P-Wave velocity structure and precise earthquake relocation at Great Sitkin Volcano, Alaska. Bull. Seismol. Soc. Am. v 98, 2428–2448.

Phillipson, G., Sobradelo, R., Gottsmann, J., 2013. Global volcanic unrest in the 21st century: an analyis of the first decade. J. Volcanol. Geotherm. Res. 264, 183–196.

Power, J.A., Stihler, S.D., White, R.A., Moran, S.C., 2004. Observations of deep long-period seismic events beneath Aleutian arc volcanoes; 1989–2002. J. Volcanol. Geotherm. Res. 138, 243–266.

Power, J.A., Stihler, S.D., Chouet, B.A., Haney, M.M., Ketner, D.M., 2013. Seismic Observations of Redoubt Volcano, Alaska 1989-2010 and a Conceptual Model of the Redoubt Magmatic System. J. Volcanol. Geotherm. Res. 259, 31–44.

Power, J.A., Friberg, P.A., Haney, M.M., Parker, T., Stihler, S.D., Dixon, J.P., 2019. A Unified Catalog of Earthquake Hypocenters and Magnitudes at Volcanoes in Alaska—1989 to 2018: U.S. Geol. Surv. Scientific Investigations Report 2019–5037, p. 17. https://doi.org/10.3133/sir20195037.

Rasmussen, D.J., Plank, T.A., Roman, D.C., Power, J.A., Bodnar, R.J., Hauri, E.H., 2018. When does eruption run-up begin? Multidisaplinary insight from the 1999 eruption of Shishaldin volcano. Earth Planet. Sci. Lett. 486, 1–14.

Roman, D.C., Cashman, K.V., 2006. The origin of volcano-tectonic earthquake swarms. Geology 34, 457–460.

Roman, D.C., Cashman, K.V., 2018. Top-down precursory volcanic seismicity: implications for stealth magma ascent and long-term eruption forecasting. Front. Earth Sci. 6, 124.

Roman, D.C., Moran, S.C., Power, J.A., Cashman, K.V., 2004. Temporal and spatial variation of local stress fields before and after the 1992 eruptions of Crater Peak vent, Mount Spurr, Alaska. Bull. Seismol. Soc. Am. 94, 2366–2379.

Roman, D.C., Rogers, M., Geirsson, H., LaFemina, P.C., Tenorio, V., 2016. Assesing the likelood and magnitude of volcanic explosions based on seismic quiescence. Earth Planet. Sci. Lett. 450, 20–28.

Roman, D.C., Soldati, A., Dingwell, D.B., Houghton, B.F., Shiro, B., 2021. Earthquakes indicated magma viscosity during Kilauea's 2018 eruption. Nature 592, 237–241.

Ruppert, N.A., Kozyreva, N.P., Hansen, R.A., 2012. Review of crustal seismicity in the Aleutian arc and implications for arc deformation. Tectonophysics 522, 150–157.

Searcy, C.K., Power, J.A., 2020. Seismic character and progression of explosive activity during the 2016-2017 eruption of Bogoslof volcano, Alaska. Bull. Volcanol. 82, 12.

Shapiro, N.M., Droznin, Droznina S. Ya, Senyukov, S.L., Gusev, A.A., Gordeev, E.I., 2017. Deep and shallow long-period volcanic seismicity linked by fluid-pressure transfer. Nat. Geosci. 10 https://doi.org/10.1038/NGEO2952.

Shelly, D.R., Hill, D.P., 2011. Migrating swarms of brttle-failure earthquakes in the lower crust beneath Mammoth Mountain, California. Geophys. Res. Lett. 38, L20307 https://doi.org/10.1029/2011GL049336.

Shelly, D.R., Hill, D.P., Massin, F., Farrell, J., Smith, R.B., Taira, T., 2013. A fluid driven earthquake swarm on the margin of Yellowstone Caldera. J. Geophys. Res. 118, 4872–4886.

Sieh, K., Natawidjaja, 2000. Neotectonics of the Sumatran fault, Indonesia. J. Geophs. Res. 105 (B12), 28295–28326.

Stix, J., de Moor, J., 2018. Understanding and forecasting Phreatic Eruptions driven by magmatic degassing. Earth Planets Space 70, 83.

Thelen, W.A., Malone, S.D., West, M.E., 2010. Respose time and cumulative moment magnitude: a new tool for forecasting eruptions. Geophys. Res. Lett. 37, L18301.

Toth, T., Kisslinger, C., 1984. Revised focal depths and velocity model for local earthquakes in the Adak seismic zone. Bull. Seismol. Soc. Am. 74, 1349–1360.
Ukawa, M., Ohtake, M., 1987. A monochromatic earthquake suggesting deep-seated magmatic activity beneath the Izu- Ooshima Volcano, Japan. J. Geophys. Res. 92, 12649–12663.
Wang, J., Lu, Z., Bekaert, D., Marshak, C., Govorcin, M., Sangha, S., Kennedy, J., Greeg, P., 2023. Along-arc volcanism in the western and central Aleutian from 2015 to 2021 revealed by cloud-based InSAR processing. Geophys. Res. Lett. m50, e2023GL106323.
Waythomas, C.F., Miller, T.P., Nye, C.J., 2003. Preliminary Volcano-Hazard Assessment for Great Sitkin Volcano, Alaska: U.S. Geol. Surv. Open-File Report 03-0112, p. 25, 1 sheet.
White, R.A., 1996. Precursory deep long-period earthquakes at Mount Pinatubo: Spatio-temporal link to a basaltic trigger. In: Newhall, C.G., Punongbayan, R.S. (Eds.), Fire and Mud: Eruptions and Lahars of Mount Pinatubo, Philippines. University of Washington Press, Seattle, pp. 307–328.
White, R.A., McCausland, W.A., 2019. A process-based model of pre-eruption seismicity patterns and its use for eruption forecasting at dormant volcanoes. J. Volcanol. Geotherm. Res. 382, 267–297.
Yang, X., Roman, D.C., Haney, M., Kupres, C.A., 2023. Double reservoirs imaged below Great Sitkin Volcano, Alaska, explain the migration of volcanic seismicity. Geophys. Res. Lett. 50 e2022GL102438.